

## Precision Intercalation of Organic Molecules in 2D Layered Materials: From Interface Chemistry to Low-Dimensional Physics

Yang Liu,<sup>§</sup> Ziren Wang,<sup>§</sup> Guoliang Hu, Xiaomeng Chen, Ke Xu, Yuqiao Guo,\* Yi Xie, and Changzheng Wu\*



Cite This: *Precis. Chem.* 2025, 3, 51–71



Read Online

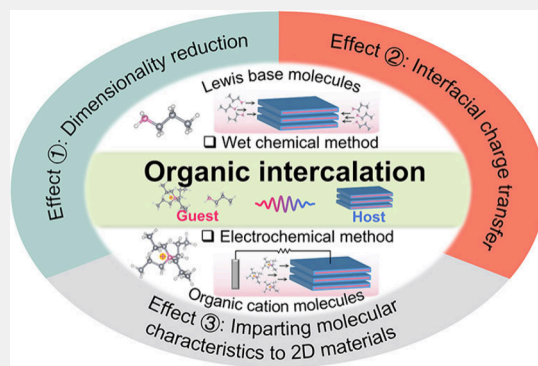
ACCESS |

Metrics & More

Article Recommendations

**ABSTRACT:** The past few decades have witnessed significant development in intercalation chemistry research aimed at precisely controlling material properties. Intercalation, as a powerful surface and interface synthesis strategy, facilitates the insertion of external guests into van der Waals (vdW) gaps in two-dimensional (2D) layered materials, inducing various modulation effects (the weakening of interlayer interactions, changes in electronic structures, interfacial charge transfer, and symmetry manipulation) to tailor material properties while preserving intralayer covalent bonds. Importantly, benefiting from the very diverse structures and properties of organic molecules, their intercalation enables the integration of various molecules with a wide array of 2D materials, resulting in the creation of numerous organic–inorganic hybrid superlattices with exotic properties, which brings extensive potential applications in fields such as spintronics, superconductor electronics, optoelectronics, and thermoelectrics. Herein, based on recent advancements in organic intercalation systems, we briefly discuss a summary and classification of various organic guest species. We also discuss three modulation effects induced by organic intercalation and further introduce intriguing modulations in physicochemical properties, including superconductivity, magnetism, thermoelectricity and thermal conductivity, chiral-induced spin selectivity (CISS) effects, and interlayer-confined chemical reaction. Finally, we offer insights into future research opportunities and emerging challenges in organic intercalation systems.

**KEYWORDS:** *intercalation chemistry, organic molecule intercalation, 2D layered materials, physicochemical property modulation, superconductivity, 2D magnetism, thermoelectricity and thermal conductivity, chiral-induced spin selectivity effect, interlayer-confined reaction*



### 1. INTRODUCTION

Engineering electronic structures in materials through surface and interfacial modification has long been a central research goal in solid-state physics, chemistry, and materials science.<sup>1–3</sup> Different from the closely packed lattice structure in many bulk solids, 2D layered materials exhibit an anisotropic structure, characterized by strong covalent bonds within atomic layers, while adjacent layers are stacked via out-of-plane weak vdW interactions, resulting in a nonbonding nature.<sup>4,5</sup> This unique structure allows the insertion of guest species, such as organic molecules, into the vdW gap between adjacent layers without disrupting the intralayer chemical bonds.<sup>6–9</sup> Consequently, the intercalation process holds enormous potential for integrating various 2D inorganic materials with diverse organic molecules, resulting in the creation of new organic–inorganic hybrid materials with tunable electronic properties. Organic intercalation offers fantastic opportunities for artificially designing novel structures and modulating electronic properties from an interface-chemistry synthesis perspective.<sup>9–11</sup>

2D layered materials exhibit a variety of intrinsic physical properties, including superconductivity, magnetism, ferroelec-

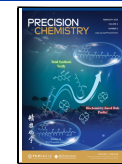
tricity, charge density waves, and topological states.<sup>12–15</sup> This diversity provides fertile ground for further chemical modulation through organic intercalation. Intercalating organic molecules can induce changes in properties—interlayer interactions,<sup>16</sup> carrier concentration,<sup>17</sup> Fermi level energy<sup>18</sup> and spin–spin interaction<sup>19</sup>—to alter and tune the intrinsic physical phenomena in 2D materials. For example, intercalating organic molecules into 2D layered superconductors can enhance their superconductivity through charge doping,<sup>20</sup> and intercalating organic molecules into 2D ferromagnets can enhance their ferromagnetic properties.<sup>21</sup> On the other hand, organic molecules are typically larger in size compared to inorganic guest species (such as metal atoms), leading to the weakening of interlayer interactions upon organic intercalation. This results in

Received: October 23, 2024

Revised: December 27, 2024

Accepted: December 30, 2024

Published: January 10, 2025



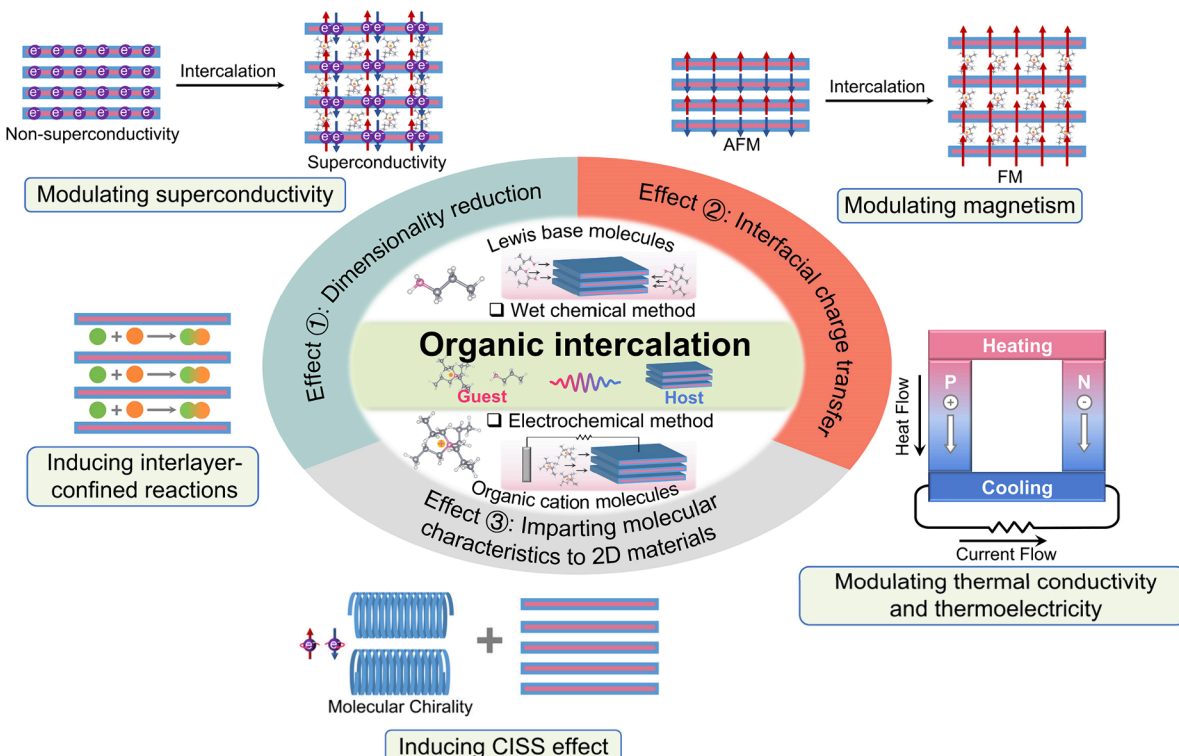


**Figure 1.** Schematic illustration of organic intercalation and its corresponding effects on the physicochemical property modulation.

decoupling of adjacent layers, giving rise to quasi-monolayer characteristics in bulk forms.<sup>16,22</sup> Overall, organic intercalation offers a powerful tool for fine-tuning the properties of 2D materials, including superconductivity, magnetism, and thermoelectricity, thereby enhancing their functionality for various applications.

Furthermore, benefiting from the almost infinite types and rich structures of organic molecules, organic intercalation has the ability to impart molecular characteristics, such as chirality,<sup>23</sup> magnetism<sup>24</sup> and hydrogen bond,<sup>25</sup> to 2D materials, thus inducing new unprecedented properties absent in the parent materials. For instance, the chiral molecular intercalation enables the creation of novel chiral solid materials and the induction of CISS effect in 2D materials, enriching their chemical functionalities;<sup>23</sup> Intercalating 1,3-diaminopropane molecules into layered SnSe<sub>2</sub> forms interfacial hydrogen bonds, introducing a new degree of freedom—interfacial hydrogen bond switch—to modulate the electrical transport properties in molecular-intercalated SnSe<sub>2</sub>.<sup>25</sup> Furthermore, organic intercalation presents new possibilities for manipulating and engineering symmetry in solid-state materials, inducing new physical phenomena.<sup>26,27</sup> For instance, the intercalation of chiral molecules with mirror symmetry breaking induces the time reversal symmetry breaking in superconducting TaS<sub>2</sub>, leading to the emergence of a novel superconducting phenomenon—chiral superconductivity.<sup>27</sup> And intercalating magnetic molecules into 2D nonmagnetic materials can produce a 2D ferromagnetic order, resulting in the magnetization of 2D nonmagnetic materials.<sup>24</sup> In addition, the vdW gaps between adjacent layers are subnanometer confined spaces, which are conductive to molecular self-assembly and interlayer-confined reactions.<sup>28,29</sup>

In this Review, we focus on the modulation of physicochemical properties of 2D materials by organic molecule intercalation, aiming to provide a guide for surface/interface engineering

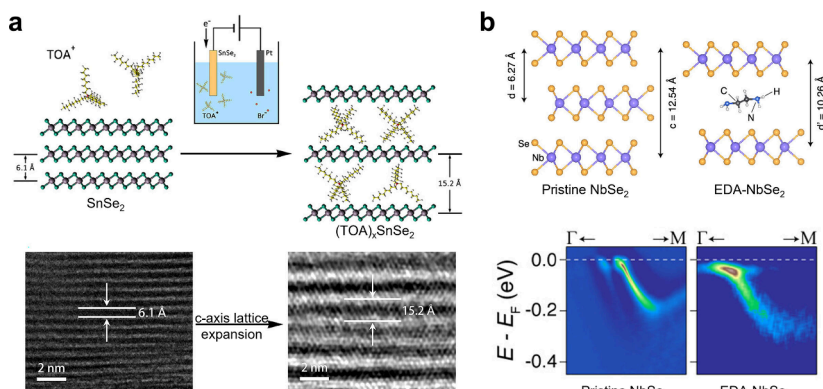
toward modulating the electronic properties. We begin with a summary of organic guest species, which can be divided into two categories: Lewis base molecules and organic cation molecules. Following this, we present the modulation effects caused by organic intercalation, which are summarized as three effects, that is, interfacial charge transfer, dimensionality reduction, and the introduction of molecular characteristics. Then, we further introduce the progress on the modulation of physicochemical properties arising from the organic intercalation, with a focus on superconductivity, magnetism, thermal conductivity and thermoelectricity, CISS effect, and interlayer-confined chemical reaction (Figure 1). Finally, we provide a brief outlook on the opportunities and challenges in the future of organic molecule intercalation in 2D materials.

## 2. INTRODUCTION OF ORGANIC GUEST SPECIES

To date, a diverse range of large-size organic molecules has been demonstrated to be intercalated into 2D materials, covering alkylamine molecules,<sup>30</sup> coordination compounds<sup>28</sup> and quaternary ammonium cations.<sup>31</sup> Generally, these diverse organic guest species can be classified into two categories (Figure 1): organic cation molecules and Lewis base molecules. The former are typically intercalated through electrochemical methods, while the latter are intercalated using wet chemical methods.<sup>10,32</sup> Electrochemical intercalation involves inserting organic ions, such as tetrabutylammonium and hexadecyltrimethylammonium cations, into 2D materials by using an electric field as a driving force in liquid or solid electrolytes. In contrast, wet chemical intercalation depends on the intrinsic electron-donating properties of Lewis base molecules to inject electrons into the host material. This results in positively charged molecules and negatively charged host materials, facilitating the insertion of organic molecules into the vdW gap space through Coulomb interactions. Notably, the intercalation of

**Table 1.** A Summary of Organic Molecules Intercalation and the Manipulation of Physicochemical Properties in 2D Materials

Organic guest species	Synthetic methods	Guest species	Host materials	Physicochemical property modulation	Years	Refs
Organic Lewis base molecules	Alkylamine molecules	Wet chemical intercalation	Pyridine	TaS <sub>2</sub>	Enhancing superconductivity	1970 <a href="#">33</a>
		Wet chemical intercalation	Chiral methylbenzylamine	TaS <sub>2</sub>	Chiral superconductivity	2024 <a href="#">27</a>
		Wet chemical intercalation	Ethylenediamine	NbSe <sub>2</sub>	Suppressing superconductivity	2023 <a href="#">16</a>
		Wet chemical intercalation	<i>n</i> -propylamine, <i>n</i> -hexylamine, <i>n</i> -octylamine and <i>n</i> -laurylamine	TaS <sub>2</sub>	Reducing thermal conductivity	2024 <a href="#">117</a>
	Coordination compounds	Wet chemical intercalation	Cobaltocene	SnS <sub>2</sub>	Room-temperature ferromagnetism	2024 <a href="#">24</a>
		Wet chemical intercalation	Cobaltocene	SnSe <sub>2</sub>	Excitonic insulator	2024 <a href="#">28</a>
	Others	Wet chemical intercalation	Tetrathiafulvalene, tetrathianaphthalene, and tetrathiadecacene	FeOCl	Altering magnetism	1987 <a href="#">37</a>
Organic cation molecules	Organic ammonium cations	Electrochemical intercalation	Tetraoctylammonium cations	SnSe <sub>2</sub>	Emerging superconductivity	2021 <a href="#">31</a>
		Electrochemical intercalation	Tetramethylammonium cations	FeSe	Enhancing superconductivity	2021 <a href="#">93</a>
		Electrochemical intercalation	Tetrabutylammonium cations	Fe <sub>3-x</sub> GeTe <sub>2</sub>	Room-temperature ferromagnetism	2023 <a href="#">21</a>
		Electrochemical intercalation	Tetraheptylammonium cations	VOCl	Room-temperature ferromagnetism	2024 <a href="#">19</a>
		Electrochemical intercalation	Tetrabutylammonium cations	VSe <sub>2</sub>	Charge density wave	2020 <a href="#">126</a>
	Imidazole cations	Electrochemical intercalation	1-Alkyl-3-methylimidazolium cations	NbSe <sub>2</sub>	Tailoring Ising superconductivity	2021 <a href="#">26</a>
		Electrochemical intercalation	1-Alkyl-3-methylimidazolium cations	MoTe <sub>2</sub> , WTe <sub>2</sub>	Enhancing superconductivity	2020 <a href="#">20</a>
		Electrochemical intercalation	1-Ethyl-3-methylimidazolium cations	FePS <sub>3</sub>	Suppressing antiferromagnetism	2024 <a href="#">109</a>

**Figure 2.** Organic intercalation-induced *c*-axis lattice expansion, leading to the dimensionality reduction effect and the monolayer properties in bulk forms. (a) Schematic illustration for the electrochemical intercalation of TOA<sup>+</sup> into SnSe<sub>2</sub>, inducing an interlayer distance increase. Reproduced from ref [31](#). Copyright 2021 American Chemical Society. (b) Schematic illustration for the EDA intercalation in NbSe<sub>2</sub>, inducing the monolayer-like band structure in EDA-NbSe<sub>2</sub>. Reproduced from ref [16](#). Copyright 2023 American Chemical Society.

Lewis base molecules are more prevalent in sulfur (S)- and selenium (Se)-based transition metal dichalcogenides (TMDs) compared with tellurium (Te)-based TMDs, mainly due to the higher electronegativity of S and Se.

In recent decades, various organic intercalants have been extensively investigated for insertion into 2D materials to modulate their physicochemical properties. As shown in Table 1, we summarize the experimental studies on organic intercalation for modulating the physicochemical properties of 2D materials. Various Lewis base molecules and organic cations have been successfully intercalated into 2D materials (Table 1). Examples of Lewis base molecules encompass alkylamine molecules (e.g., pyridine,<sup>33</sup> ethylamine,<sup>30</sup> ethylenedi-

amine<sup>16,30,34</sup>), amide molecules (e.g., formamide<sup>35</sup>) and coordination compounds (e.g., cobaltocene<sup>28</sup>), and others (e.g., tetrathiafulvalene<sup>36,37</sup>). Organic cations include organic ammonium cations,<sup>31,38,39</sup> and organic imidazole cations.<sup>26</sup> These organic species can be introduced into a variety of 2D materials to fine-tune their physicochemical properties, including superconductivity,<sup>16,26,27</sup> magnetism,<sup>21,24,40</sup> and thermoelectricity.<sup>41,42</sup> Furthermore, organic intercalation can induce unique physical phenomena absent in the parent host material, such as tailoring Ising superconductivity.<sup>26</sup> Notably, in addition to the above-mentioned small molecules, polymers can also be inserted into interlayer vdW space through ion exchange<sup>43–45</sup> and interlayer-confined synthesis.<sup>46</sup>

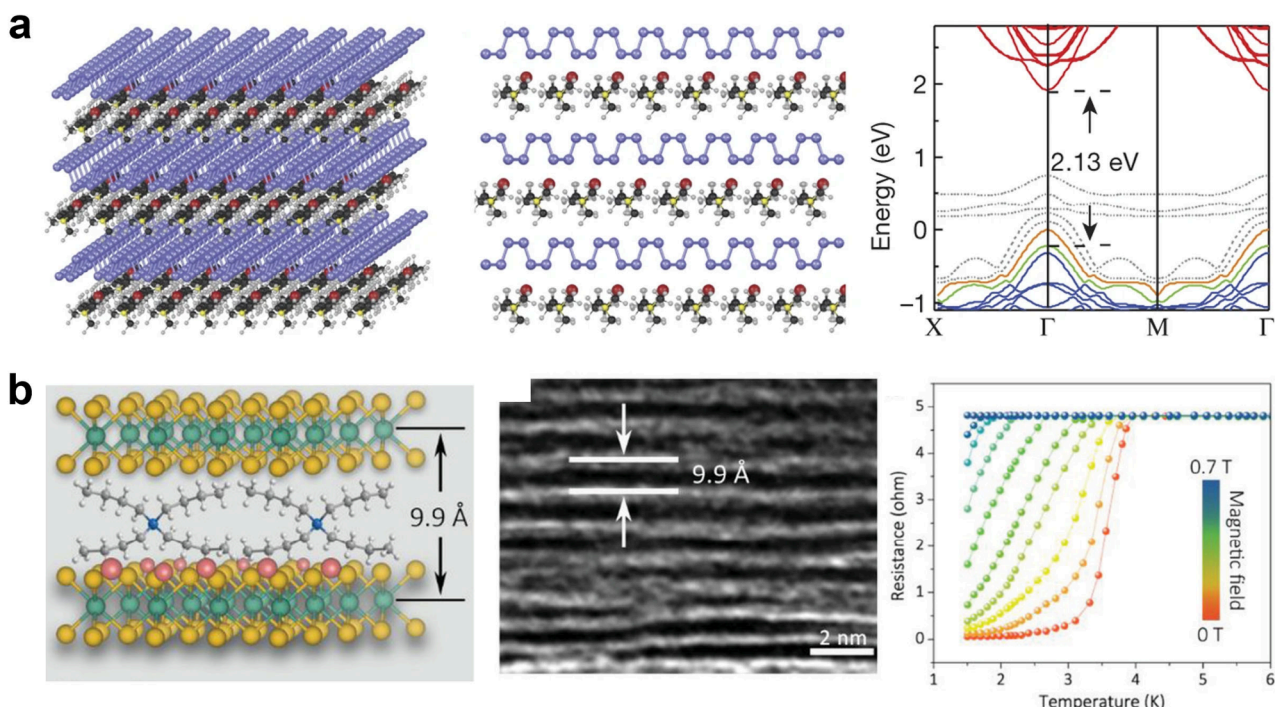


**Figure 3.** Interlayer distance expansion leads to modulation of the electronic properties. (a) Schematic illustration for the intercalation of  $\text{CTA}^+$  into black phosphorus, realizing the monolayer atomic crystal molecular superlattice. Reproduced from ref 22. Copyright 2018 Springer Nature. (b) Schematic illustration for the intercalation of  $\text{TBA}^+$  in  $\text{TaS}_2$ , enhancing its superconductivity with a  $T_c$  of  $\sim 3.8$  K. Reproduced from ref 52. Copyright 2020 Wiley.

### 3. EFFECTS OF ORGANIC INTERCALATION

The introduction of organic cations/molecules into the vdW gaps can lead to alterations in various material attributes, such as interlayer interactions, carrier concentration, Fermi-level energy, electronic structure, symmetry breaking, and spin–spin exchange interactions. These changes are a result of the intercalation effects triggered by the insertion of organic intercalants, ultimately altering and modulating the physicochemical properties of the 2D materials. In this section, we provide a brief overview and discussion of these intercalation effects including dimensionality reduction, interfacial charge transfer, and the introduction of molecular characteristics.

#### 3.1. Dimensionality Reduction

Dimensionality reduction is a key consequence of the intercalation of organic guest species into the interlayer space. Different from metallic atoms,<sup>47–49</sup> organic guest species often have large size, whose intercalation trigger the interlayer expansion. For example, the electrochemical intercalation of tetraoctylammonium ions ( $\text{TOA}^+$ ) into  $\text{SnSe}_2$  leads to the interlamellar spacing increasing from 6.1 to 15.2 Å, as shown in Figure 2a.<sup>31</sup> Notably, when the molecular size is substantially larger, the interlayer spacing can expand multiple times, or even tens of times, compared to its original distance, such as the intercalation of cetyltrimethylammonium cations ( $\text{CTA}^+$ ), octadecylamine molecules or stearamide molecules.<sup>50,51</sup>

This  $c$ -axis lattice expansion can weaken the interlayer interaction, resulting in the decoupling of adjacent inorganic layers and causing them to behave as monolayer effects.<sup>16,26,52</sup> Consequently, organic intercalation can induce the emergence of monolayer-like properties in bulk forms.<sup>22,53,54</sup> An illustrative example is the ethylenediamine (EDA) intercalation in  $\text{NbSe}_2$  (the top panel of Figure 2b), where the interlayer coupling is

reduced, resulting in the emergence of an electronic structure closely resembling that of monolayer  $\text{NbSe}_2$ .<sup>16</sup> The angle-resolved photoemission spectroscopy (ARPES) measurements reveal that the splitting of Nb 4d-derived bands near the Fermi level is present in pristine bulk  $\text{NbSe}_2$ , whereas it disappears in EDA intercalated  $\text{NbSe}_2$ , as shown in the bottom panel of Figure 2b. This observation in EDA- $\text{NbSe}_2$  is consistent with the band structure of monolayer  $\text{NbSe}_2$ .<sup>55</sup>

Due to interlayer decoupling and dimensionality reduction, organic intercalation can lead to a variety of changes, including adjustments to bandgap values,<sup>22,39</sup> electronic structures,<sup>18,28</sup> and flexibility.<sup>42,56</sup> For example, the electrochemical intercalation of  $\text{CTA}^+$  in black phosphorus produces molecular superlattices that exhibit the intrinsic properties of monolayer phosphorene (the left and middle panels of Figure 3a).<sup>22</sup> After  $\text{CTA}^+$  intercalation, the bandgap value in this molecular superlattice increases to 2.13 eV (the right panel of Figure 3a). Furthermore, certain properties of layered materials show dimensionality-dependent characteristics, such as the bandgap in  $\text{MoS}_2$ ,<sup>57</sup> magnetic properties in A-type antiferromagnets,<sup>58–60</sup> and the superconducting temperatures in  $\text{TaS}_2$ .<sup>52,61</sup> Consequently, the dimensionality reduction effect triggered by organic intercalation can alter and tune these intrinsic electronic properties, giving rise to intriguing physical phenomena. For instance, the intercalation of tetrabutylammonium ions ( $\text{TBA}^+$ ) into  $\text{TaS}_2$  enhances superconductivity, achieving a critical temperature ( $T_c$ ) of  $\sim 3.8$  K (Figure 3b), which represents the highest  $T_c$  reported for monolayer  $\text{TaS}_2$ .<sup>52</sup> This enhancement is primarily attributed to electronic decoupling between adjacent  $\text{TaS}_2$  layers, caused by organic intercalation. In  $\text{TaS}_2$ , the impact of dimensionality reduction on  $T_c$  values outweighs that of electron doping.<sup>11,61,62</sup>

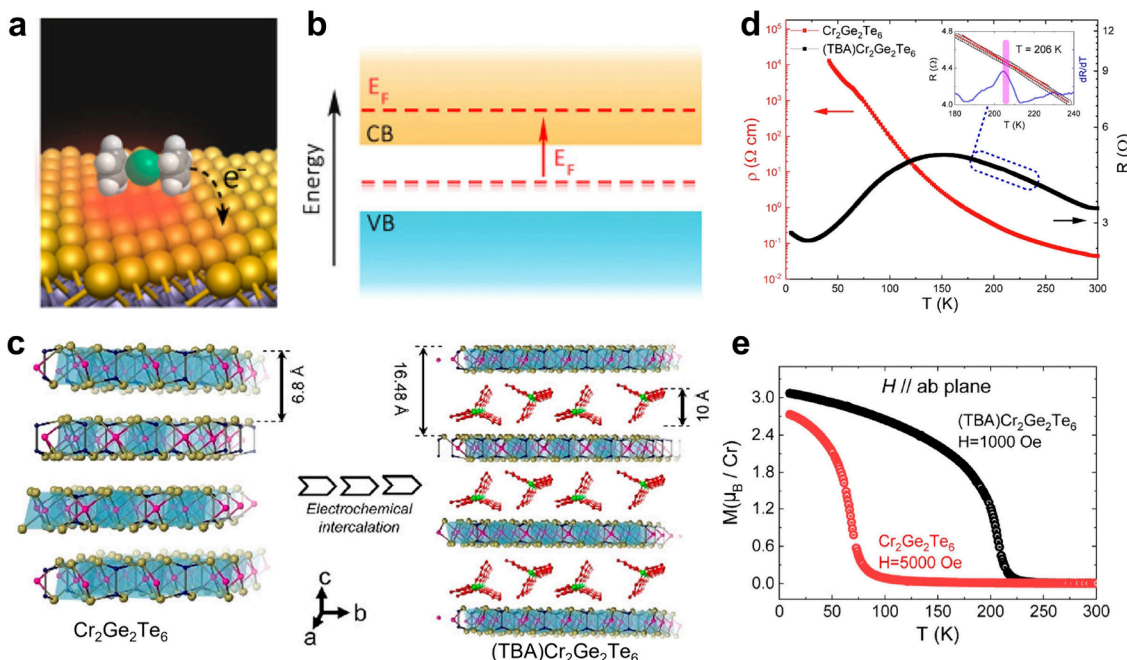


**Figure 4.** Organic intercalation-induced interfacial charge transfer effect. (a) Schematic illustration for interfacial charge transfer from  $\text{Co}(\text{Cp})_2$  to  $\text{SnSe}_2$  in the  $\text{Co}(\text{Cp})_2$ -intercalated  $\text{SnSe}_2$  superlattice. (b) Schematic illustration for the shift of  $E_F$  caused by  $\text{Co}(\text{Cp})_2$  intercalation in  $\text{SnSe}_2$ . (a,b) Reproduced from ref 18. Copyright 2017 American Chemical Society. (c) Schematic illustration for the electrochemical intercalation of  $\text{TBA}^+$  in  $\text{Cr}_2\text{Ge}_2\text{Te}_6$ . (d) Temperature-dependent electrical transport of  $\text{Cr}_2\text{Ge}_2\text{Te}_6$  and  $(\text{TBA})\text{Cr}_2\text{Ge}_2\text{Te}_6$ . (e) Temperature-dependent magnetic susceptibilities of  $\text{Cr}_2\text{Ge}_2\text{Te}_6$  and  $(\text{TBA})\text{Cr}_2\text{Ge}_2\text{Te}_6$ . (c–e) Reproduced from ref 73. Copyright 2019 American Chemical Society.

Intriguingly, the role of organic intercalation in reducing interlayer interactions can be effectively utilized in the exfoliation of layered materials to produce atomically thin (monolayer or few-layer) nanosheets.<sup>63–65</sup> In particular, the electrochemical intercalation of organic cations presents a robust “top-down” method for obtaining 2D nanomaterials.

Additionally, organic intercalation-induced interlayer spacing expansion can decrease the energy barrier for alkali metal ion diffusion, thus improving energy storage capabilities.<sup>66–70</sup> For example, intercalating organic molecules (such as triethylene glycol and tetrahydrofuran) into 2D ultrathin  $\text{VOPO}_4$  nanosheets can greatly improve sodium ion transport properties and, consequently, enhance the sodium ion storage capabilities.<sup>66</sup> Furthermore, organic intercalation allows for the integration of diverse organic molecules with various 2D materials, resulting in the formation of organic-2D materials heterointerfaces.<sup>2,51,71</sup> These 2D hybrid heterointerfaces lead to interfacial lattice mismatch, interfacial phonon scattering and high anisotropy, opening up new opportunities for modulating thermal conductivity and thermoelectricity.<sup>72</sup>

### 3.2. Interfacial Charge Transfer

The interfacial charge transfer between organic intercalants and host 2D materials is another critical consequence of organic intercalation. With the insertion of positively charged Lewis base molecules or organic cations into the interlayer space, electrons are injected into the inorganic layers to maintain electrical neutrality, resulting in the appearance of an interfacial charge transfer. This interfacial charge transfer effect is a prevalent phenomenon in intercalated compounds, offering an ideal avenue for electron doping without disrupting the in-plane structure.

Organic intercalation-induced interfacial charge transfer plays a crucial role in changing material properties, such as altering carrier concentration, shifting Fermi levels, and modifying

electronic structures. These alterations, in turn, alter and modulate various electronic properties of 2D materials, including electronic phase transitions,<sup>18,73</sup> magnetism<sup>19,40</sup> and superconductivity.<sup>38,74</sup> In the case of layered semiconductors, organic intercalation drives electrons to occupy the conduction band, leading to a shift of Fermi level ( $E_F$ ), and facilitating an electronic phase transition from a semiconducting to a metallic states, as shown in Figure 4a,b.<sup>18</sup> Observations of such electronic transitions have been revealed in certain organic-inorganic hybrid superlattices, such as organic-intercalated  $\text{SnSe}_2$ <sup>18,31,38</sup> and  $\text{Cr}_2\text{Ge}_2\text{Te}_6$ .<sup>73</sup> For example, the intercalation of  $\text{TBA}^+$  into  $\text{Cr}_2\text{Ge}_2\text{Te}_6$  triggers an electronic transition from its original semiconductor phase to a metallic state (Figure 4c,d).<sup>73</sup> Meanwhile, its ferromagnetic properties undergo alterations and enhancements, evidenced by an increase in the Curie temperature from 67 to 208 K (Figure 4e) and a switch in the magnetic axis orientation from along the C-axis to within the ab plane. This phenomenon results from the electron injection into unoccupied  $d_{xz}$  and  $d_{yz}$  orbitals of Cr and a change in spin–spin exchange mechanism from superexchange to double exchange. Additionally, the transition temperature ( $T_c$ ) in superconductors is closely related to carrier concentration.<sup>75,76</sup> Organic intercalation-induced interfacial charge transfer effect can alter the carrier concentration, resulting in the modulation of superconductivity in layered superconductors, especially the  $T_c$  values.<sup>20,77</sup> The manipulation of superconductivity through organic intercalation will be discussed in detail in Section 4.1.

Intriguingly, organic-intercalated-induced interfacial charge transfer can induce the separation of electrons and holes and the generation of a built-in electric field at the organic-2D material heterointerfaces. This phenomenon, in turn, leads to the emergence of the quantum-confined Stark effect, which offers an innovative approach for electrically manipulating interlayer excitons and obtaining excitonic insulators.<sup>28,78–80</sup> A prominent

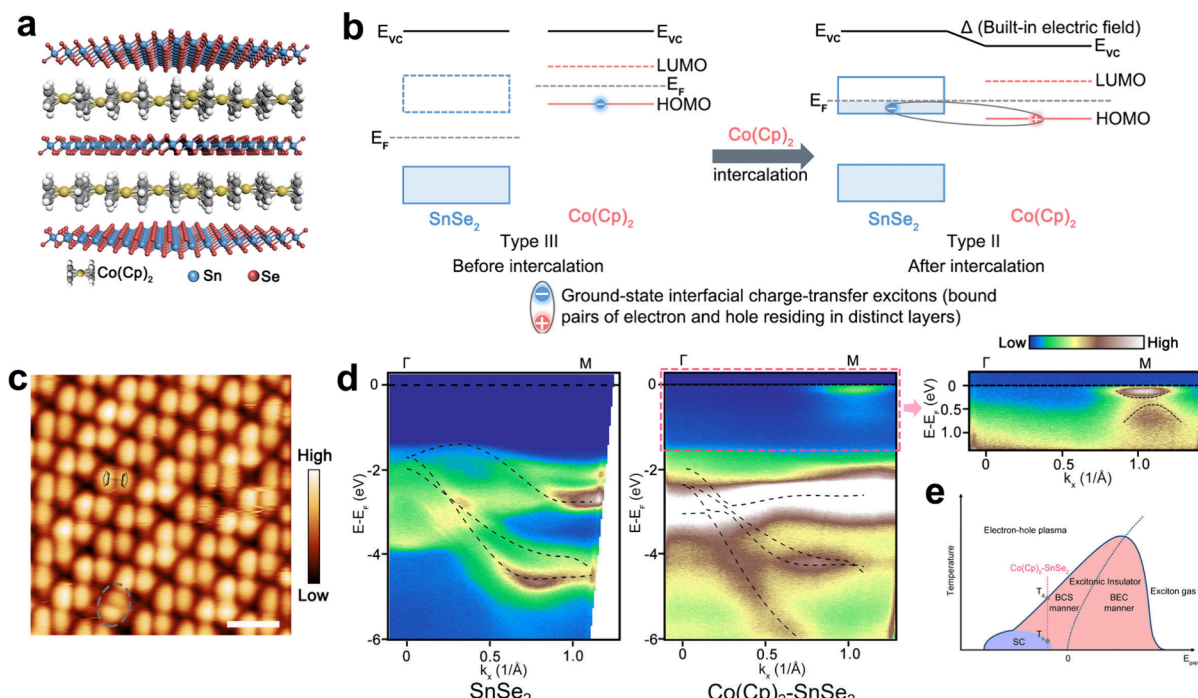


**Figure 5.** Organic intercalation-induced quantum-confined Starks effect for achieving excitonic insulators. (a) Model diagram of the  $\text{Co}(\text{Cp})_2$ -intercalated  $\text{SnSe}_2$  superlattice structure. (b) Schematic illustration for interfacial quantum Starks effect in the  $\text{Co}(\text{Cp})_2$ - $\text{SnSe}_2$  superlattice from the perspective of interface energy level alignment. (c) Scanning tunneling microscopy (STM) image of the exposed  $\text{Co}(\text{Cp})_2$  layer in the  $\text{Co}(\text{Cp})_2$ - $\text{SnSe}_2$  superlattice. (d) Electronic band structures of the  $\text{SnSe}_2$  crystal and  $\text{Co}(\text{Cp})_2$ - $\text{SnSe}_2$  superlattice measured by ARPES. (e) Phase transitions of  $\text{Co}(\text{Cp})_2$ - $\text{SnSe}_2$  superlattice in phase diagram of excitonic insulator as delineated by red dotted line. (a–e) Reproduced from ref 28. Copyright 2024 American Chemical Society.

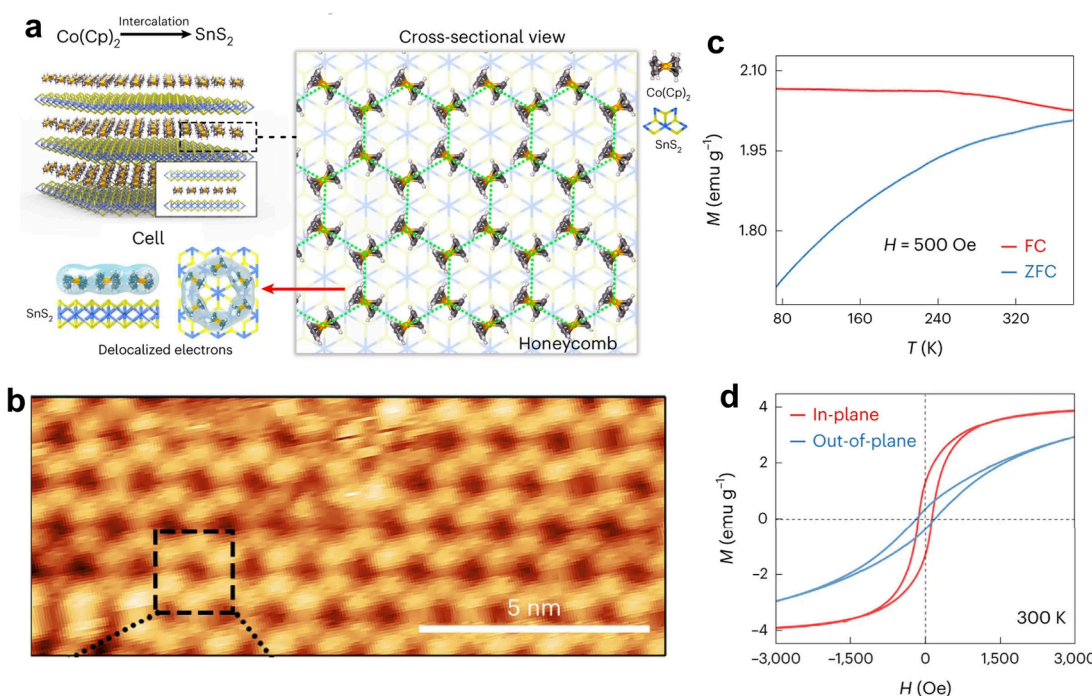


**Figure 6.** Magnetizing 2D nonmagnetic materials via organic intercalation. (a) Schematic illustration for the  $\text{Co}(\text{Cp})_2$ -intercalated  $\text{SnS}_2$  superlattice structure. (b) Constant-current STM image of a monolayer of  $\text{Co}(\text{Cp})_2$  on  $\text{SnS}_2$ . (c) Temperature-dependent magnetic susceptibility of a  $\text{Co}(\text{Cp})_2$ -intercalated  $\text{SnS}_2$  superlattice under a magnetic field of 500 Oe. (d) Anisotropic isothermal magnetization curves at 300 K. (a–d) Reproduced from ref 24. Copyright 2024 Springer Nature.

example of this phenomenon is the self-assembly intercalation of cobaltocene ( $\text{Co}(\text{Cp})_2$ ) molecules in  $\text{SnSe}_2$ , resulting in the formation of a novel interfacial charge transfer excitonic

insulator, as shown in Figure 5a,e.<sup>28</sup>  $\text{Co}(\text{Cp})_2$  molecules with 19 valence electrons exhibit intrinsic electron-donating properties, and their intercalation triggers the electron transfer from the

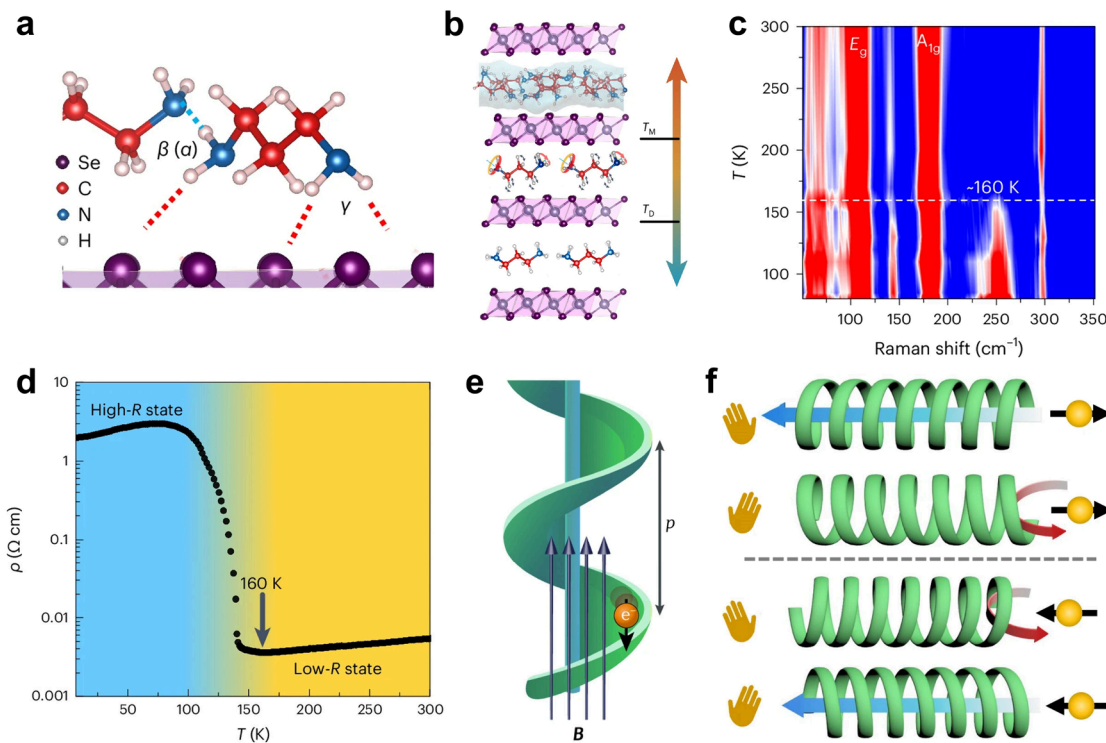


**Figure 7.** Organic intercalation-induced introduction of molecular characteristics into 2D materials. (a) Schematic illustration for interfacial hydrogen bonds in the 1,3-DAP-intercalated SnSe<sub>2</sub> superlattice. (b) Schematic illustration for the (1,3-DAP)<sub>0.5</sub>SnSe<sub>2</sub> superlattice structure. (c) Temperature-dependent Raman spectra of (1,3-DAP)<sub>0.5</sub>SnSe<sub>2</sub>. (d) Temperature-dependent resistivity ( $\rho$ ) of (1,3-DAP)<sub>0.5</sub>SnSe<sub>2</sub>. (a–d) Reproduced from ref 25. Copyright 2024 Springer Nature. (e) Schematic illustration for charge polarization of chiral molecules. Reproduced from ref 85. Copyright 2024 Springer Nature. (f) Schematic illustration for acting spin filter. Reproduced from ref 23. Copyright 2022 Springer Nature.

highest occupied molecular orbital (HOMO) of Co(Cp)<sub>2</sub> to the conduction band of SnSe<sub>2</sub>. Furthermore, after Co(Cp)<sub>2</sub> intercalation, the establishment of an interfacial built-in electric field prompts the HOMO of Co(Cp)<sub>2</sub> to shift downward into the band gap of SnSe<sub>2</sub>, as shown in Figure 5b. The intramolecular conjugated structure and the intermolecular ordered assembly structure (Figure 5c) facilitate the discrete energy level to form an energy band, leading to the introduction of an extra valence band belonging to Co(Cp)<sub>2</sub> molecules into the bandgap of SnSe<sub>2</sub> (Figure 5d). Consequently, Co(Cp)<sub>2</sub> intercalation enables the construction of a unique band structure, comprising an electron conduction and hole valence bands separated by a narrow band gap conducive to electron–hole pairing. In the Co(Cp)<sub>2</sub>-intercalated SnSe<sub>2</sub> superlattice, experimental features were observed, including a narrow excitonic gap, formation of a charge density wave without periodic lattice distortion, exitonic gap opening, and metal–insulator transition. These experimental observables serve as direct evidence of excitonic insulators, highlighting the strong interplay between 2D materials layers and molecular layers.

### 3.3. Imparting Molecular Characteristics to 2D Materials

Organic molecules possess diverse electronic and structural characteristics, such as molecular magnetism, chirality, and hydrogen bonds. Upon intercalation of organic molecules, these molecular attributes can be imparted to 2D materials, presenting new possibilities for manipulating the electronic properties of 2D materials. Through the integration of 2D materials with suitable molecules, the material properties can be altered and modulated, such as symmetry and intermolecular force, resulting in the emergence of novel physical properties absent in the parent bulk materials. These novel physical properties include

unconventional superconductivity,<sup>26,27</sup> 2D molecular ferromagnetism,<sup>24</sup> CISS effects,<sup>23,81</sup> and metal–insulator transitions.<sup>25</sup>

The discovery of new 2D ferromagnetic materials is crucial for both fundamental research and technological applications.<sup>13</sup> Compared to magnetic materials, nonmagnetic materials are still the majority. The intercalation of magnetic molecules, which provide the source of localized magnetic moments, provides a versatile strategy to magnetize nonmagnetic materials and enrich the family of 2D magnetic materials. A prominent example is the observation of 2D room-temperature ferromagnetism in Co(Cp)<sub>2</sub>-intercalated SnS<sub>2</sub> superlattice.<sup>24</sup> As a typical nonmagnetic layered metal chalcogenide, SnS<sub>2</sub> provides a confined space within its interlayer vdW gaps, which can restrict the geometric and spin orientation of Co(Cp)<sub>2</sub> molecules. By employing wet chemical methods for intercalating Co(Cp)<sub>2</sub> molecules into SnS<sub>2</sub>, a novel organic–inorganic (Co(Cp)<sub>2</sub>/SnS<sub>2</sub>) superlattice structure is synthesized (Figure 6a), wherein Co(Cp)<sub>2</sub> molecules form a honeycomb-like structure with delocalized  $\pi$ -bond electron distribution (Figure 6b). Magnetic measurements (Figure 6c,d) reveal the existence of ferromagnetism in confined Co(Cp)<sub>2</sub> monolayers, exhibiting a high Curie temperature exceeding the range limit of the instrument (380 K) and an in-plane easy magnetic axis.

Hydrogen bonds are ubiquitous in organic compounds and biological structures.<sup>82</sup> Molecular intercalation can introduce such weak intermolecular interaction into organic–inorganic hybrid superlattices, offering a new avenue—interfacial hydrogen bonds (Figure 7a)—to modulate electronic properties. For instance, intercalating 1,3-diaminopropane (1,3-DAP) molecules in SnSe<sub>2</sub> forms interfacial hydrogen bonds (Figure 7b), allowing control over the metal–insulator transition by the

**Table 2.** A Summary of Organic Molecules Intercalation for Modulating Superconductivity (SC)

Categories	Organic molecules	Host materials	Refs	Notes
Modulating $T_c$ values	Emerging SC in non-SC materials	Tetraoctylammonium cations Cetyltrimethylammonium and tetraethylammonium cation	$\text{SnSe}_2$ $\text{MoS}_2$	31 74
	Enhancing intrinsic SC	Pyridine 1-Alkyl-3-methylimidazolium cations	$\text{TaS}_2$ $\text{MoTe}_2$ , $\text{WTe}_2$	33 20
	Suppressing intrinsic SC	Ethylenediamine Aniline	$\text{NbSe}_2$ $\text{NbS}_2$	16 88
Manipulating symmetry breaking	Inversion symmetry breaking	1-Alkyl-3-methylimidazolium cations	$\text{NbSe}_2$	26
	Time-reversal symmetry breaking	Right-/left-handed methylbenzylamine	$\text{TaS}_2$	27

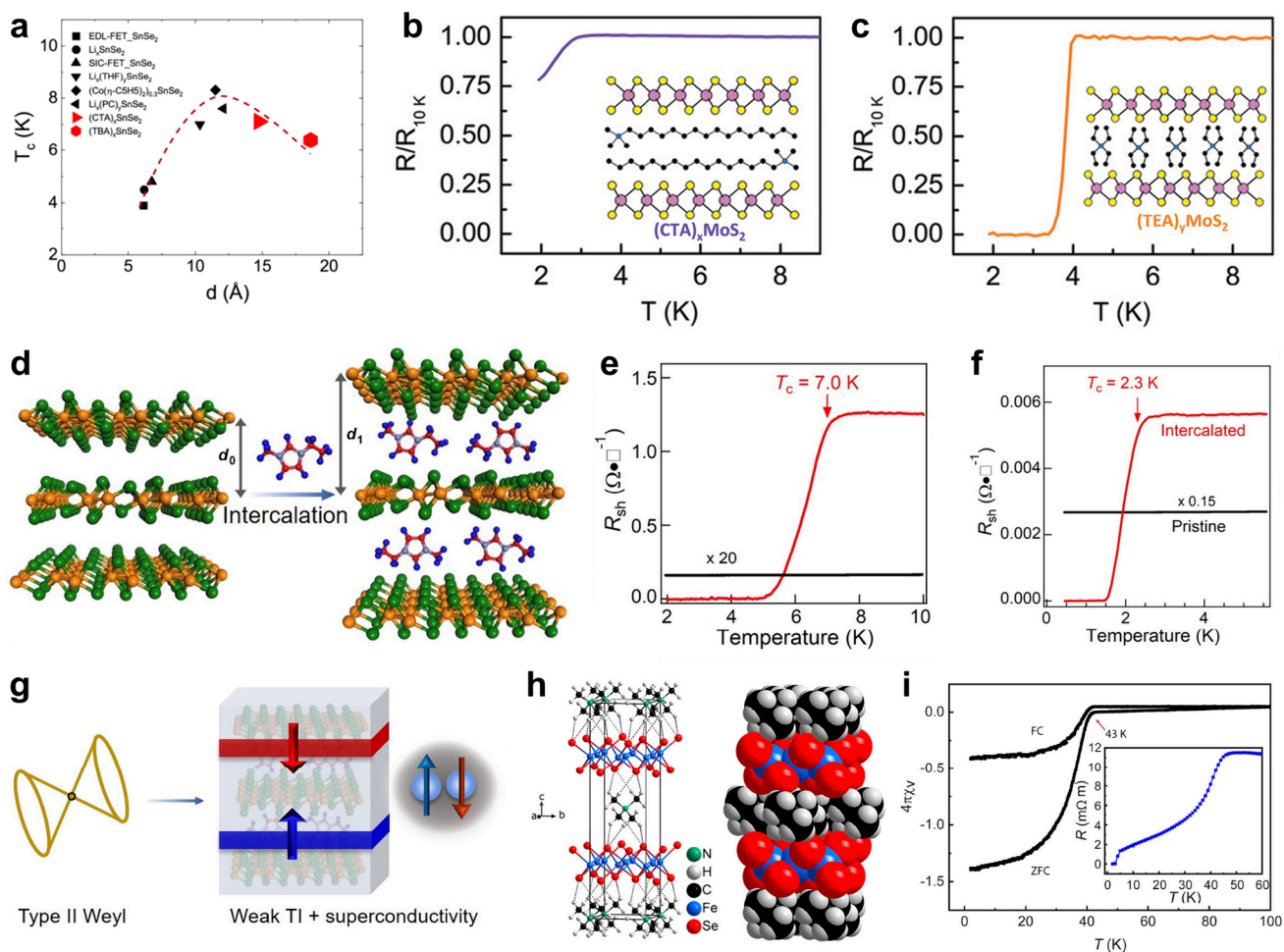


**Figure 8.** Organic intercalation modulates  $T_c$  values in 2D superconductors. (a) A summary of guest-intercalation-induced superconductivity in  $\text{SnSe}_2$ . Reproduced from ref 38. Copyright 2020 American Physical Society. (b,c) Resistance of  $\text{CTA}^+$ - and  $\text{TEA}^+$ -intercalated  $\text{MoS}_2$  in the low-temperature range, respectively. Reproduced from ref 74. Copyright 2022 Wiley. (d) Schematic illustration for the intercalation of imidazolium cations into  $\text{MoTe}_2$ . (e) Resistance of pristine  $\text{MoTe}_2$  and imidazolium-ion-intercalated  $\text{MoTe}_2$  in the low-temperature range. (f) Resistance of pristine  $\text{WTe}_2$  and imidazolium-ion-intercalated  $\text{WTe}_2$  in the low-temperature range. (g) Schematic illustration for the emergence of superconducting weak topological insulators from Weyl semimetals  $\text{MoTe}_2$  and  $\text{WTe}_2$  through organic intercalation. (d–g) Reproduced from ref 20. Available under a CC-BY Creative Commons Attribution 4.0 International license (<https://creativecommons.org/licenses/by/4.0/>). Copyright 2020, published by Elsevier. (h,i) Schematic illustration and superconducting magnetic measurements of  $\text{TMA}^+$ -intercalated  $\text{FeSe}$ . Reproduced from ref 93. Copyright 2021 American Chemical Society.

dynamic-static switch of hydrogen bonds.<sup>25</sup> Within the confined vdW space, the temperature-triggered alteration in self-rotation properties of amino ( $-\text{NH}_2$ ) groups induces the transition of the hydrogen bonds from dynamic to static states. At moderate temperatures, the  $-\text{NH}_2$  groups self-rotate spontaneously to

form transient hydrogen bonds, inducing a dynamic charge-delocalized mode with high electronic conductivity. Conversely, at low temperature, the self-rotation of  $-\text{NH}_2$  groups ceases, leading to the formation of static hydrogen bonds that are detectable by Raman (Figure 7c). This transition shifts to a

charge-localized mode with a lower electronic conductivity. This switch of hydrogen bonds occurs around the critical temperature of  $\sim 160$  K, resulting in a metal–insulator transition with a high on–off ratio of up to  $10^7$ , as shown in Figure 7d.

In addition, it has been demonstrated that chiral molecules can be intercalated into layered crystals to obtain chiral solid materials.<sup>23,81,83–85</sup> The chirality in organic molecules originates from mirror symmetry breaking, a fundamental molecular property, which can induce charge-to-spin conversion arising from charge polarization of chiral molecules (Figure 7e). This results in the CISS effect, which serves as a spin filter for electron transport (Figure 7f). The CISS effect in nonmagnetic chiral materials will be discussed in detail in Section 4.4. Additionally, intercalating chiral molecules can manipulate the symmetry breaking, leading to the emergence of chiral superconductivity,<sup>27</sup> as discussed in detail in Section 4.1.

#### 4. PHYSICOCHEMICAL PROPERTY MODULATION VIA ORGANIC INTERCALATION

Recently, very diverse organic intercalation systems have been successfully developed to modulate the physicochemical properties and enhance the functionalities in 2D materials. It is worth highlighting that in organic intercalation systems the modulation of the physicochemical properties, typically requires multiple intercalation effects (as mentioned in Section 3 above) to simultaneously alter material properties, rather than relying on just one effect to affect electronic properties.

Organic intercalation offers a powerful tool to alter and manipulate intrinsic physicochemical properties, giving rise to the development of new physical phenomena not present in the parent bulk materials. In this section, we will provide a brief overview of recent advancements in modulating physicochemical properties through organic intercalation, with a focus on the superconductivity, magnetism, thermal conductivity, thermoelectricity, and CISS effects. Additionally, we will also mention interlayer confinement reactions within the vdW gap, highlighting the impact of subnanoscale spaces on enabling precise control of chemical reactions.

##### 4.1. Superconductivity Properties

Superconductivity, the first macroscopic quantum phenomenon discovered, is a pivotal subject in modern condensed matter physics.<sup>86</sup> Research on the modulation of superconductivity through organic intercalation has a rich history dating back to the 1970s.<sup>30,33,87</sup> In 1970, pyridine-intercalated  $\text{TaS}_2$  became the first organic-intercalated superconductor, demonstrating an enhancement of superconductivity.<sup>33</sup> This groundbreaking discovery paved the way for similar findings in other organic-intercalated superconductors. In 2D superconducting materials, organic molecules intercalation can effectively modulate their superconducting properties, particularly the alteration in the superconducting  $T_c$  value.<sup>16,20,77,88</sup> Furthermore, organic intercalation has the potential to manipulate and engineer symmetry breaking, such as inversion symmetry breaking<sup>26</sup> and time-reversal symmetry breaking,<sup>27</sup> thus inducing the emergence of unconventional superconducting behaviors. Accordingly, in the following, we briefly summarize and introduce the superconductivity modulation through organic intercalation from two aspects: modulating  $T_c$  values and manipulating symmetry breaking (Table 2).

**4.1.1. Modulating  $T_c$  Values.** The study of modulating  $T_c$  values in layered superconductors has attracted widespread attention. The intercalation of organic molecules can weaken

interlayer electronic coupling and facilitate charge injection, thereby altering the electronic structure and carrier concentration in 2D materials, and further modulating their superconductivity. Overall, this phenomenon can be categorized into three distinct types: the introduction of superconductivity in nonsuperconducting host materials, the enhancement of intrinsic superconductivity, and the suppression of intrinsic superconductivity (Table 2).

In certain layered nonsuperconducting materials, such as  $\text{SnSe}_2$ ,  $\text{TiSe}_2$ ,  $\text{MoS}_2$  and  $\text{MoSe}_2$ , the interfacial charge transfer induced by organic intercalation can lead to the emergence of superconductivity.  $\text{SnSe}_2$  serves as the most representative material, in which charge doping through electronic gating or chemical intercalation facilitates the transition from a semiconductor to a superconducting state, as shown in Figure 8a. For example, the chemical intercalation of  $\text{TOA}^+$ ,  $\text{TBA}^+$ , hexadecyltrimethylammonium ions ( $\text{CTA}^+$ ) and  $\text{Co}(\text{Cp})_2$  can induce the emergence of superconductivity in  $\text{SnSe}_2$ . Beyond  $\text{SnSe}_2$ , Pereira et al. intercalated  $\text{MoS}_2$  with  $\text{CTA}^+$  and tetraethylammonium ( $\text{TEA}^+$ ) cations, leading to the observation of superconducting onset temperature of 2.8 and 3.9 K, respectively, as shown in Figure 8b,c.<sup>74</sup>

Then, in certain layered superconductors, such as  $\text{TaS}_2$ ,  $\text{T}_d\text{-MoTe}_2$  and  $\text{T}_d\text{-WTe}_2$ , organic intercalation can enhance their superconducting properties. These layered materials typically exhibit relatively low  $T_c$  values, such as 0.8 K for bulk 2H- $\text{TaS}_2$ , 0.25 K for bulk  $\text{T}_d\text{-MoTe}_2$ , and 0.82 K for monolayer  $\text{WTe}_2$  (the bulk counterpart is nonsuperconducting). Following organic molecule intercalation, their  $T_c$  values markedly increase. In 1970, Gamble et al. first reported the enhancement of superconductivity in pyridine-intercalated  $\text{TaS}_2$ .<sup>33</sup> Notably, in organic-intercalated  $\text{TaS}_2$  superlattices, the superconductivity enhancement originates from both the charge transfer and dimensionality reduction, with the latter playing a more significant role.<sup>11,52,62,89</sup> A similar enhancement is observed in layered Weyl semimetals  $\text{T}_d\text{-MoTe}_2$  and  $\text{T}_d\text{-WTe}_2$ .<sup>20</sup> Employing electrochemical intercalation techniques to inserting imidazolium ions into  $\text{MoTe}_2$  and  $\text{WTe}_2$  (Figure 8d) achieves superconducting states with  $T_c$  values of 7.0 and 2.3 K, respectively (Figure 8e,f). This enhancement is attributed to the charge transfer effect, which increases the density of states near the Fermi level. Notably, this approach also leads to the formation of a superconducting weak topological insulator (Figure 8g). The integration of superconductivity into topological phases holds promise for applications in quantum computing.

Intriguingly, in high-temperature superconductors, their superconducting temperatures are typically closely related to carrier concentration.<sup>17,75,76,90–92</sup> The interfacial charge transfer effect from organic intercalation can alter the carrier concentration, thus significantly increasing the  $T_c$  values in Fe-based superconductors.<sup>77,93,94</sup> For example, the  $T_c$  values in  $\text{FeSe}$  can be increased through the electrochemical intercalation of organic cations, as shown in Figure 8h,i. Intercalating tetramethylammonium ( $\text{TMA}^+$ ),<sup>93</sup>  $\text{CTA}^+$ ,<sup>77</sup> and  $\text{TBA}^+$ <sup>94</sup> cations into  $\text{FeSe}$  results in high-temperature superconducting states with  $T_c$  values of 43, 45, and 50 K, respectively. Compared to the intrinsic  $T_c$  of  $\sim 8$  K, the superconducting properties in these intercalated  $\text{FeSe}$  atoms are significantly improved.

Finally, in certain hole-type superconducting materials, organic intercalation can weaken and even suppress the intrinsic superconducting properties. For example, 2H- $\text{NbSe}_2$  and 2H- $\text{NbS}_2$  are representative materials.<sup>54</sup> When EDA molecules are

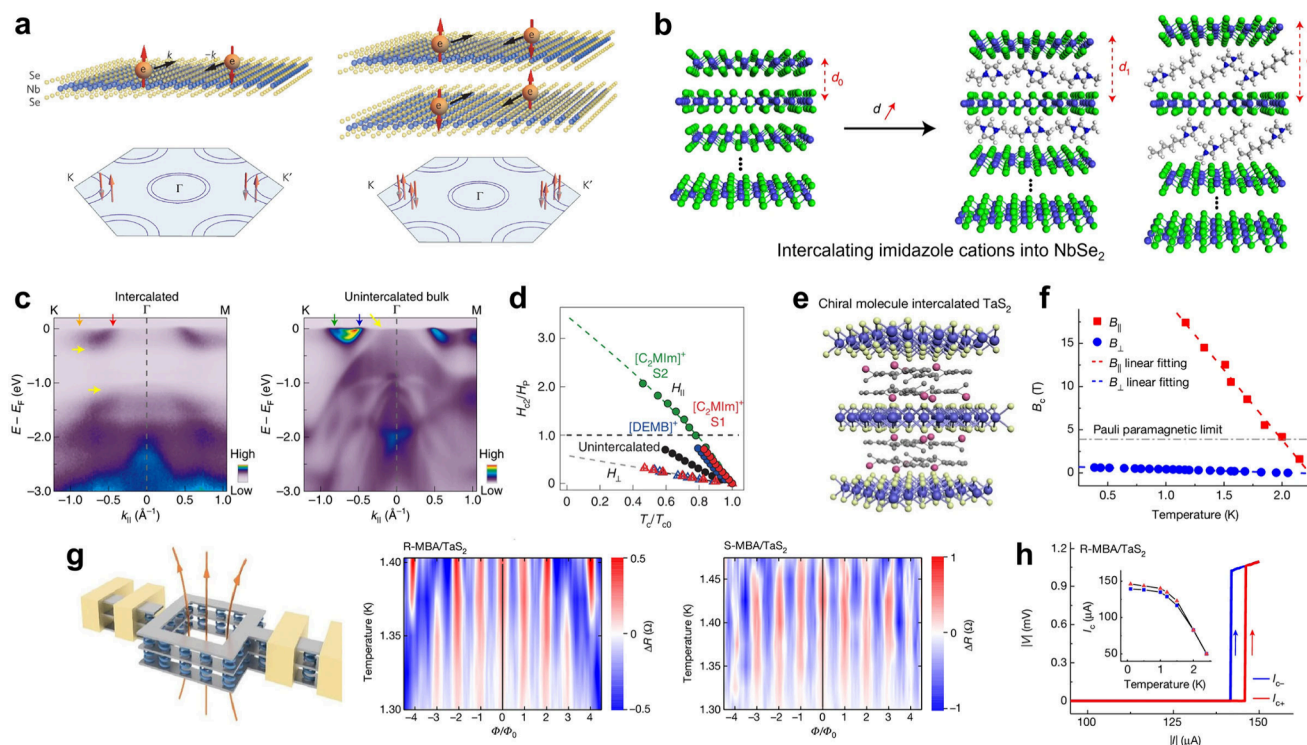


**Figure 9.** Organic intercalation manipulates symmetry breaking for unconventional superconductivity. (a) Schematic illustration for spin-momentum locking in monolayer (left) and bilayer/bulk (right)  $\text{NbSe}_2$ . Reproduced from ref 97. Copyright 2015 Springer Nature. (b) Schematic drawing for the intercalation of imidazole cations into  $\text{NbSe}_2$ . (c) Band structures of intercalated  $\text{NbSe}_2$  (left panel) and pristine  $\text{NbSe}_2$  (right panel) measured by ARPES. (d) Upper critical magnetic fields  $H_{c2}$  for out-of-plane magnetic fields ( $H_{\perp}$ ) and in-plane magnetic fields ( $H_{\parallel}$ ) as a function of temperature. (b–d) Reproduced from ref 26. Copyright 2022 Springer Nature. (e) Schematic illustration for the superlattice structure of R-MBA- and S-MBA-intercalated 2H-TaS<sub>2</sub>. (f) Upper critical magnetic fields for out-of-plane magnetic fields ( $B_{c2,\perp}$ ) and in-plane magnetic fields ( $B_{c2,\parallel}$ ) as a function of temperature. (g) Little-Parks measurements, showing a robust  $\pi$  phase shift. (h) Absolute value of voltage–current characteristics for R-MBA-intercalated 2H-TaS<sub>2</sub> measured at 0.5 K. (e–h) Reproduced from ref 27. Copyright 2024 Springer Nature.

inserted into  $\text{NbSe}_2$ , the original superconductivity with a  $T_c$  of  $\sim 6$  K is suppressed. This intercalated structure exhibits normal metallic behavior at the lowest tested temperature of 2 K, without any superconducting transition. A similar weakening can be observed in aniline, pyridine, picoline- and EDA-intercalated  $\text{NbS}_2$  compounds.<sup>88</sup> This observation is similar to the weakening and suppression of superconductivity that occurs through the intercalation of metal ions into the  $\text{NbS}_2$  or  $\text{NbSe}_2$  systems.<sup>47</sup>

**4.1.2. Manipulating Symmetry Breaking for Novel Superconductivity.** Manipulating and engineering symmetry in solid-state materials has the potential to induce novel physical phenomena.<sup>95,96</sup> For example, inversion symmetry breaking can trigger spin–orbit physics and unconventional Ising superconductivity. Organic intercalation presents a promising method for altering this symmetry in 2D materials. Recently, Zhang et al. demonstrated that the effectiveness of organic intercalation in manipulating inversion symmetry breaking in bulk 2H-NbSe<sub>2</sub>, leading to the emergence of Ising superconductivity.<sup>26</sup> This superconducting phenomenon is typically observed in some monolayer H-phase TMDs, with noncentrosymmetric crystalline structure that exhibits intrinsic inversion symmetry breaking and mirror symmetry.<sup>97–99</sup> This unique structure exhibits spin-momentum locking (Figure 9a), which locks the spin to the out-of-plane direction, resulting in exceptionally high in-plane upper critical fields exceeding the Pauli paramagnetic limit ( $H_p$ ), corresponding to Ising superconductivity. Interestingly, such Ising superconductivity was

successfully observed in bulk  $\text{NbSe}_2$  with organic cation intercalation (Figure 9b).<sup>26</sup> Inserting organic cations (1-alkyl-3-methylimidazolium ions) increases the interlayer spacing from  $\sim 6.2$  to  $10.1$  Å, effectively reducing the dimensionality of  $\text{NbSe}_2$  and achieving monolayer properties, as demonstrated by ARPES (Figure 9c). Magneto-electrical transport measurements reveal that the intercalated  $\text{NbSe}_2$  exhibits remarkably high in-plane upper critical fields surpassing the Pauli paramagnetic limit, indicating unique Ising superconductivity properties that are not present in bulk  $\text{NbSe}_2$  (Figure 9d). This study highlights the potential of organic intercalation strategies to enhance the noncentrosymmetric properties of monolayers, enabling symmetry manipulation.

Additionally, the intercalation of chiral molecules in noncentrosymmetric superconductors has the potential to manipulate time-reversal symmetry breaking, leading to the realization of chiral superconductivity.<sup>27,100,101</sup> Specifically, through a wet chemical method, right-handed methylbenzylamine (R-MBA) and left-handed methylbenzylamine (S-MBA) have been intercalated into 2H-TaS<sub>2</sub>, resulting in the artificial creation of novel chiral organic–inorganic hybrid superlattices (Figure 9e).<sup>27</sup> In this chiral superlattice, several key unconventional superconducting features were observed: (1) an anomalously large in-plane upper critical field (Figure 9f), far exceeding the Pauli paramagnetic limit; (2) a robust  $\pi$  phase shift in Little-Parks measurements (Figure 9g), indicating the presence of unconventional pairing symmetry; and (3) a field-free superconducting diode effect (Figure 9h), signifying the breaking of

**Table 3.** A Summary of Organic Molecule Intercalation for Modulating Magnetic Properties

Categories		Organic molecules	Host materials	Refs	Notes
2D magnetic materials	Enhancing intrinsic ferromagnetic properties in 2D ferromagnetic materials	Tetrabutylammonium cations	$\text{Fe}_{3-x}\text{GeTe}_2$	21	Room-temperature ferromagnetism
	Transforming antiferromagnetism into ferromagnetism	Tetrabutylammonium cations	$\text{Cr}_2\text{Ge}_2\text{Te}_6$	73	
		Tetraheptylammonium cations	$\text{NiPS}_3$	112	
		Tetraheptylammonium cations	VOCl	19	Room-temperature ferromagnetism
	Magnetizing 2D nonmagnetic materials	Cobaltocene	$\text{SnS}_2$	24	Room-temperature ferromagnetism

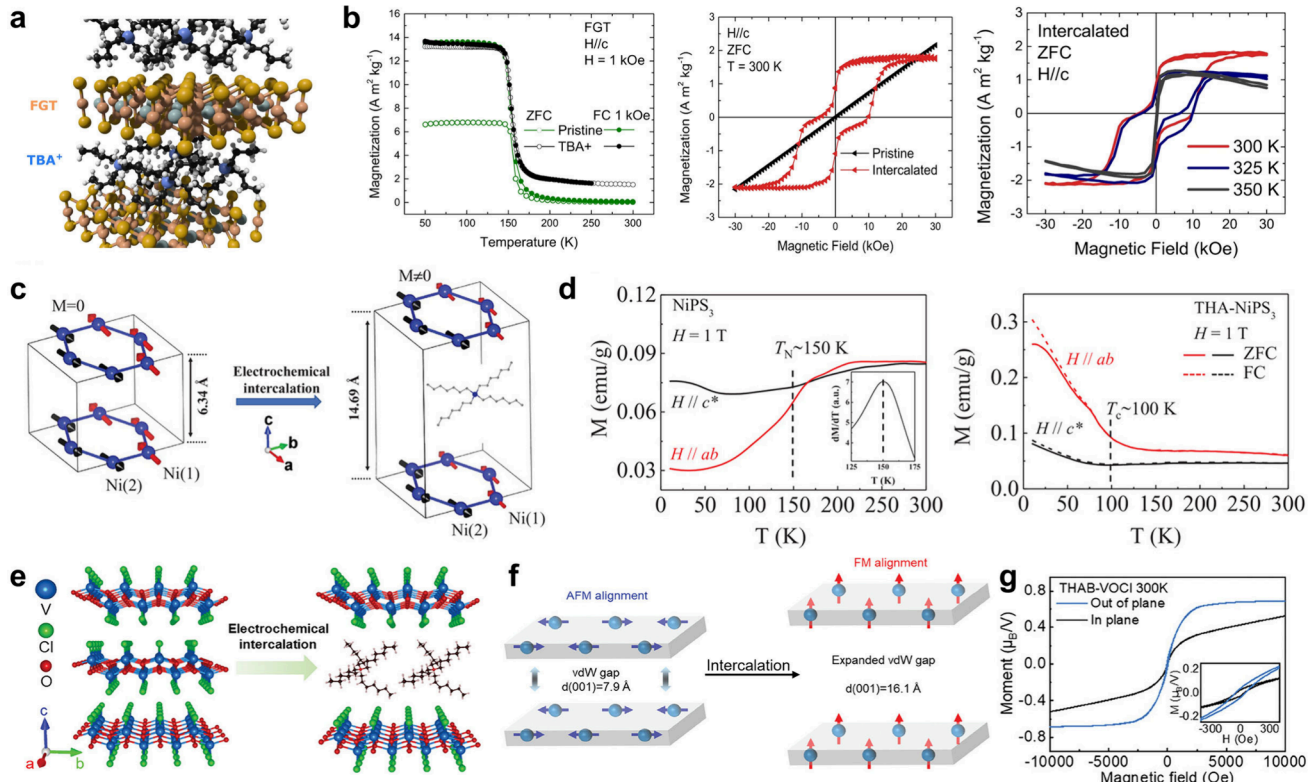


**Figure 10.** Organic intercalation modulates the intrinsic magnetic properties in 2D ferromagnetic and antiferromagnetic materials. (a) Schematic illustration for the superlattice structure of  $\text{TBA}^+$ -intercalated  $\text{Fe}_{3-x}\text{GeTe}_2$ . (b) Magnetic measurements in  $\text{TBA}^+$ -intercalated  $\text{Fe}_{3-x}\text{GeTe}_2$  and pristine  $\text{Fe}_{3-x}\text{GeTe}_2$ : zero-field-cooled (ZFC, open symbols) and field-cooled (FC, solid symbols) curves (left panel) and the isothermal magnetic-field-dependent magnetization ( $M$ – $H$ ) at 300 K (middle panel) and at various temperatures (right panel). (a,b) Reproduced from ref 21. Available under a CC-BY Creative Commons Attribution 4.0 International license (<https://creativecommons.org/licenses/by/4.0/>). Copyright 2023, The Authors, published by Springer Nature. (c) Schematic illustration for the magnetic structure transformation from antiferromagnetism in pristine  $\text{NiPS}_3$  (left) to ferrimagnetism in  $\text{THA}^+$ -intercalated  $\text{NiPS}_3$  (right). (d) ZFC and FC curves of pristine  $\text{NiPS}_3$  (left) and  $\text{THA}^+$ -intercalated  $\text{NiPS}_3$ , (c,d) Reproduced from ref 112. Copyright 2022 Wiley. (e) Schematic illustration for the electrochemical intercalation of  $\text{VOCl}$  with  $\text{THA}^+$ . (f) Schematic illustration for the transformation of spin–spin interaction from A-type antiferromagnetism in pristine  $\text{VOCl}$  to ferromagnetism in  $\text{THA}^+$ -intercalated  $\text{VOCl}$ . (g)  $M$ – $H$  curves for  $\text{THA}^+$ -intercalated  $\text{VOCl}$  under the in-plane and out-of-plane fields at 300 K, exhibiting room-temperature ferromagnetism. (e)–(g) Reproduced from ref 19. Copyright 2024 Wiley.

time-reversal symmetry in the superconducting state. These experimental features are absent in the pristine  $\text{TaS}_2$  crystal, suggesting the presence of unconventional chiral superconductivity in the chiral superlattice. This presents distinctive opportunities for manipulating symmetry, modulating topological states and exploring exotic physical properties.

#### 4.2. Magnetic Properties

In 2017, the experimental study on  $\text{CrI}_3$ <sup>102</sup> and  $\text{Cr}_2\text{Ge}_2\text{Te}_6$ <sup>103</sup> successfully demonstrated the existence of long-range ferromagnetic order in 2D lattices, overcoming the limitations of Mermin–Wagner theorem.<sup>104</sup> This breakthrough discovery has

sparked significant interest in 2D ferromagnetic materials, which are crucial for the development of innovative, low-power, high-density spintronics devices in the future.<sup>105,106</sup> However, the limited availability of 2D ferromagnetic materials and their relatively low Curie temperatures have hindered further research and application. Organic intercalation offers a versatile tool for altering and improving the magnetic properties in 2D materials. Through organic intercalation strategies, it is possible to manipulate the intrinsic magnetism of 2D materials (Table 3), including both ferromagnetic and antiferromagnetic properties, resulting in a higher ferromagnetic Curie temperature or a

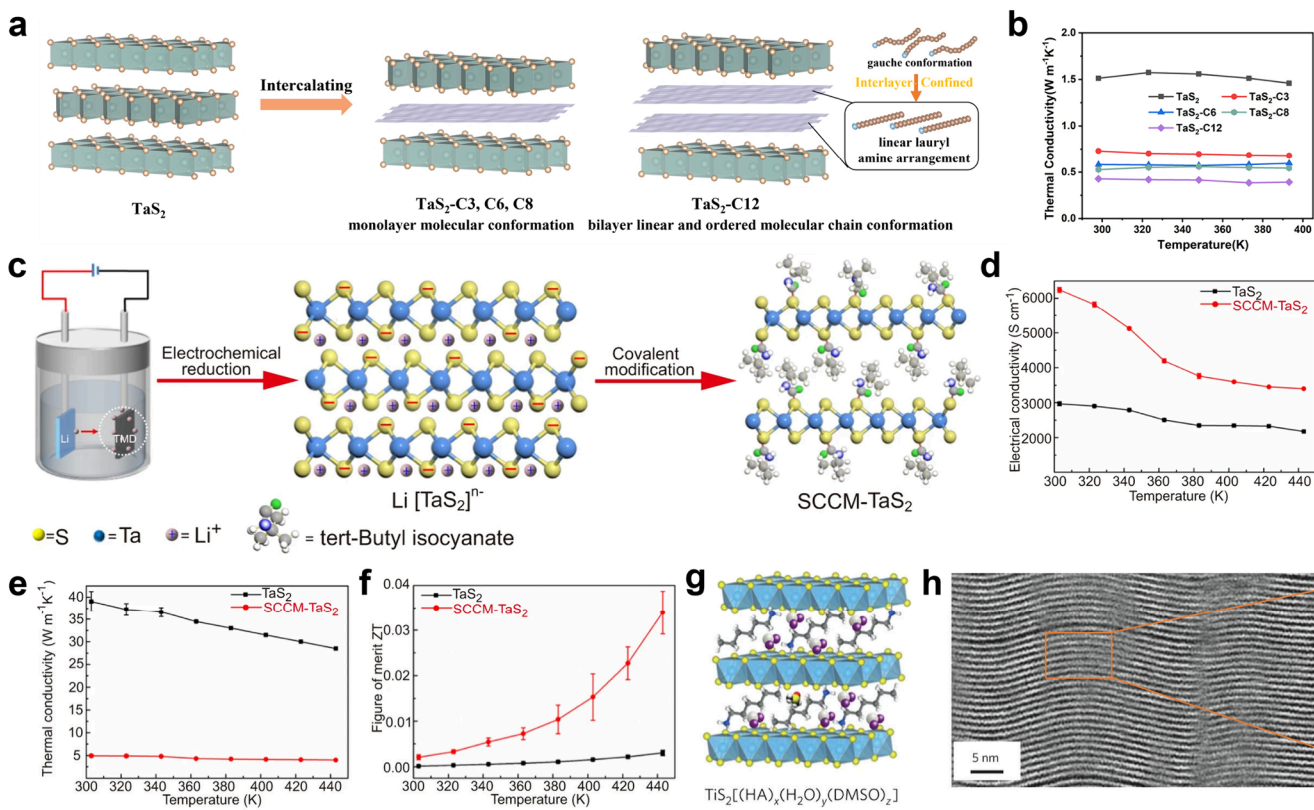


**Figure 11.** Organic intercalation modulates thermal conductivity and thermoelectric properties. (a) Schematic illustration for the intercalation of monolayer and bilayer alkylamine molecules in  $\text{TaS}_2$ , showing tunable interlayer spacing and molecular configuration for thermal conductivity modulation. (b) Temperature dependence of the total thermal conductivity of  $\text{TaS}_2$ ,  $\text{TaS}_2\text{-C}3$ ,  $\text{TaS}_2\text{-C}6$ ,  $\text{TaS}_2\text{-C}8$  and  $\text{TaS}_2\text{-C}12$ . (a,b) Reproduced from ref 117. Copyright 2024 Science China Press. (c) Schematic illustration for synthesis processes of side chains covalent modification  $\text{TaS}_2$  (SCCM- $\text{TaS}_2$ ). (d)–(f) Thermoelectric properties of the pristine  $\text{TaS}_2$  and SCCM- $\text{TaS}_2$ : electrical conductivity (d), in-plane thermal conductivity (e), and in-plane thermoelectric ZT (f). (c)–(f) Reproduced from ref 41. Available under a CC-BY Creative Commons Attribution 4.0 International license (<https://creativecommons.org/licenses/by/4.0/>). Copyright 2022, The Authors, published by Springer Nature. (g) Schematic illustration for the superlattice structure of organic intercalation  $\text{TiS}_2$ . (h) Cross-sectional high-angle annular dark-field scanning transmission electron microscopy (HAADF-STEM) image of the organic intercalation  $\text{TiS}_2$  superlattice. (g,h) Reproduced from ref 42. Copyright 2015 Springer Nature.

transformation from antiferromagnetism to ferromagnetism.<sup>19,21</sup> Additionally, organic intercalation enables the magnetization of 2D nonmagnetic materials (Table 3), introducing external 2D ferromagnetic order into 2D nonmagnetic materials, and thereby creating novel artificial magnetic materials.<sup>24</sup> This approach can broaden the 2D ferromagnetic material family and opens up new possibilities for research and applications in 2D magnetic materials.

First, organic intercalation can modulate the intrinsic magnetic properties in 2D materials.<sup>10,11,32,107–110</sup> In recent years, various 2D magnetic layered materials with ordered magnetic structures have been discovered, such as ferromagnetic  $\text{Cr}_2\text{Ge}_2\text{Te}_6$ ,  $\text{VSe}_2$ ,  $\text{Fe}_3\text{GeTe}_2$ ,  $\text{Fe}_5\text{GaTe}_2$  and  $\text{CrBr}_3$ , and antiferromagnetic  $\text{CrI}_3$ ,  $\text{MnBi}_2\text{Te}_4$ ,  $\text{CrSBr}$ ,  $\text{VOCl}$ ,  $\text{FePS}_3$ ,  $\text{MnPS}_3$  and  $\text{NiPS}_3$ . Intercalating organic molecules effectively alters their intrinsic magnetic structures, which can be categorized into two aspects: enhancing the original ferromagnetic properties and transforming “technologically useless” antiferromagnetism into “useful” ferromagnetism. For the former, Iturriaga et al. reported the enhancement of ferromagnetic properties in layered ferromagnetic  $\text{Fe}_{3-x}\text{GeTe}_2$  through  $\text{TBA}^+$  intercalation.<sup>21</sup> The electrochemical intercalation of  $\text{TBA}^+$  into  $\text{Fe}_{3-x}\text{GeTe}_2$  (Figure 10a) improves intrinsic ferromagnetic properties, raising the Curie temperature from  $\sim 154$  to  $\sim 350$  K, thereby achieving 2D room-temperature

ferromagnetism, as demonstrated by magnetic measurements (Figure 10b). This enhancement is attributed to the charge injection effect induced by organic intercalation. A similar enhancement can be observed in  $\text{TBA}^+$ -intercalated  $\text{Cr}_2\text{Ge}_2\text{Te}_6$  (Figure 4c), with a significant alteration of the original ferromagnetic properties, including an increase in Curie temperature from  $\sim 67$  to  $\sim 208$  K (Figure 4e) and a change in the easy magnetization axis from along the *c*-axis to within the *ab*-plane.<sup>73,111</sup>

In 2D antiferromagnetic materials, organic intercalation has the ability to modify their original antiferromagnetic structures, leading to the emergence of ferromagnetic order, including room-temperature ferromagnetism.<sup>19,40,107,109,112</sup> The electrochemical intercalation of tetraheptylammonium ions ( $\text{THA}^+$ ) in  $\text{NiPS}_3$  can transform the original zigzag antiferromagnetic structure into a ferrimagnetic structure, as shown in Figure 10c,d.<sup>112</sup> Additionally, the antiferromagnetic properties of  $\text{NiPS}_3$  can be modulated by the intercalation of  $\text{TBA}^+$  ions<sup>40</sup> and imidazolium<sup>109</sup> ions. Notably, among the various antiferromagnetic structures, A-type antiferromagnetism is distinguished by its unique magnetic structure, characterized by intralayer ferromagnetic coupling and interlayer antiferromagnetic coupling.<sup>58–60</sup> This magnetic structure is closely related to the interlayer interaction, making it possible to modulate magnetism through organic intercalation. For

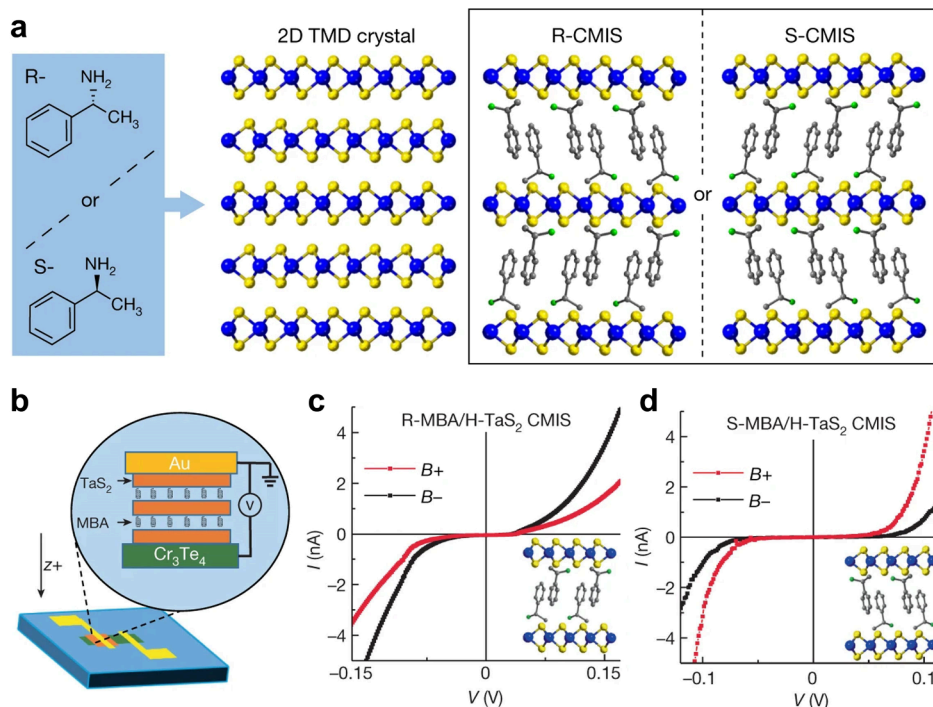


**Figure 12.** Chiral molecule intercalation artificially creates chiral solid-state materials, resulting in CISS effect. (a) Schematic drawings for the preparation of chiral molecular intercalation superlattices (CMIS) through the intercalation of R-MBA and S-MBA chiral molecules in TaS<sub>2</sub>. (b) Schematic drawing for a typical spin tunnelling junction device, which CMIS serves as the spin-filtering layer. (c,d)  $I$ – $V$  curves of R-MBA- and S-MBA-intercalated TaS<sub>2</sub> CMIS at 10 K, respectively. (a)–(d) Reproduced from ref 23. Copyright 2022 Springer Nature.

example, the electrochemical intercalation of THA<sup>+</sup> in A-type antiferromagnetic VOCl can convert antiferromagnetism to room-temperature ferromagnetism (Figure 10e).<sup>19</sup> This transformation is achieved by increasing the interlayer spacing with THA<sup>+</sup> intercalation, weakening interlayer interactions and suppressing original interlayer antiferromagnetic coupling (Figure 10f). Accompanied by the simultaneous electron doping effect, which enhances the intralayer ferromagnetic coupling, THA<sup>+</sup> intercalation induces the emergence of room-temperature ferromagnetism (Figure 10g) and the switch in the easy magnetization axis from in-plane to out-of-plane.

In addition, organic intercalation can magnetize 2D non-magnetic materials, leading to the introduction of external long-range magnetic structures.<sup>24</sup> The vdW gaps provide a rigid confinement environment conducive to the self-assembly of magnetic molecules, forming novel 2D molecular ferromagnets. For instance, the self-assembly intercalation of molecular magnets (magnetic Co(Cp)<sub>2</sub> molecules) in SnS<sub>2</sub> has been demonstrated to induce 2D room-temperature ferromagnetism (Figure 6), as discussed in the Section 3.3.<sup>24</sup> Besides Co(Cp)<sub>2</sub>-intercalated SnS<sub>2</sub>, Coronado et al.<sup>113</sup> employed a synthetic strategy involving exfoliation and reassembly to integrate negatively charged monolayers of TaS<sub>2</sub> with single-molecule magnet layers. This approach successfully achieved the coexistence of superconductivity and single-molecule magnet layers, enriching the functionalities of 2D inorganic materials.

#### 4.3. Thermal Conductivity and Thermoelectricity Properties

Thermoelectric technology has the ability to realize direct conversion between thermal and electrical energy, whose development hinge on the efficient manipulation of the transport behaviors of electrons and phonons.<sup>114,115</sup> The heat to electrical energy conversion performance is quantified by the

dimensionless figure of merit, ZT. This is defined using the formula  $ZT = \sigma S^2 T / (\kappa_e + \kappa_l)$ , where  $\sigma$ ,  $S$ ,  $T$ ,  $\kappa_e$  and  $\kappa_l$  are the electrical conductivity, the Seebeck coefficient, absolute temperature, the electronic thermal conductivity and the lattice thermal conductivity, respectively.<sup>114,115</sup> Apparently, high-performance thermoelectric materials need a combination of large electrical conductivity, low thermal conductivity, and a large Seebeck coefficient. However, these parameters are strongly interdependent and coupled with each other, making it challenging to improve ZT values. To this end, various modulation strategies have been developed to address this, including defect chemistry<sup>115,116</sup> and intercalation chemistry.<sup>10,41,42</sup> Among these, organic intercalation has proven to be an effective method for enhancing the thermoelectric performance in 2D materials. Specifically, intercalating organic molecules into 2D materials creates organic-2D materials hybrid interfaces, affecting interfacial phonon scattering and reducing thermal conductivity. Furthermore, organic intercalation triggers the interfacial charge transfer effect, altering the carrier concentration and ultimately improving electrical conductivity.

Importantly, organic intercalation produces tunable interlayer spacing and molecular configuration, providing new degrees of freedom for thermal conductivity modulation. For example, Wang et al.<sup>117</sup> reported the intercalation of monolayer and bilayer molecules into TaS<sub>2</sub>, leading to a dramatic reduction in thermal conductivity. In several alkylamine-intercalated TaS<sub>2</sub> superlattices (propyl amine, hexylamine, octylamine, and lauryl amine), increasing the length of the intercalated alkyl chain (C<sub>3</sub>, C<sub>6</sub>, C<sub>8</sub>, and C<sub>12</sub>) leads to a more ordered and linear configuration of the alkyl chain, while the gauche conformation decreases. Notably, C<sub>12</sub>-intercalated TaS<sub>2</sub> forms a bilayer linear molecular chain, whereas C<sub>3</sub>-, C<sub>6</sub>-, and C<sub>8</sub>-intercalated TaS<sub>2</sub> retain a molecular monolayer structure between TaS<sub>2</sub> layers

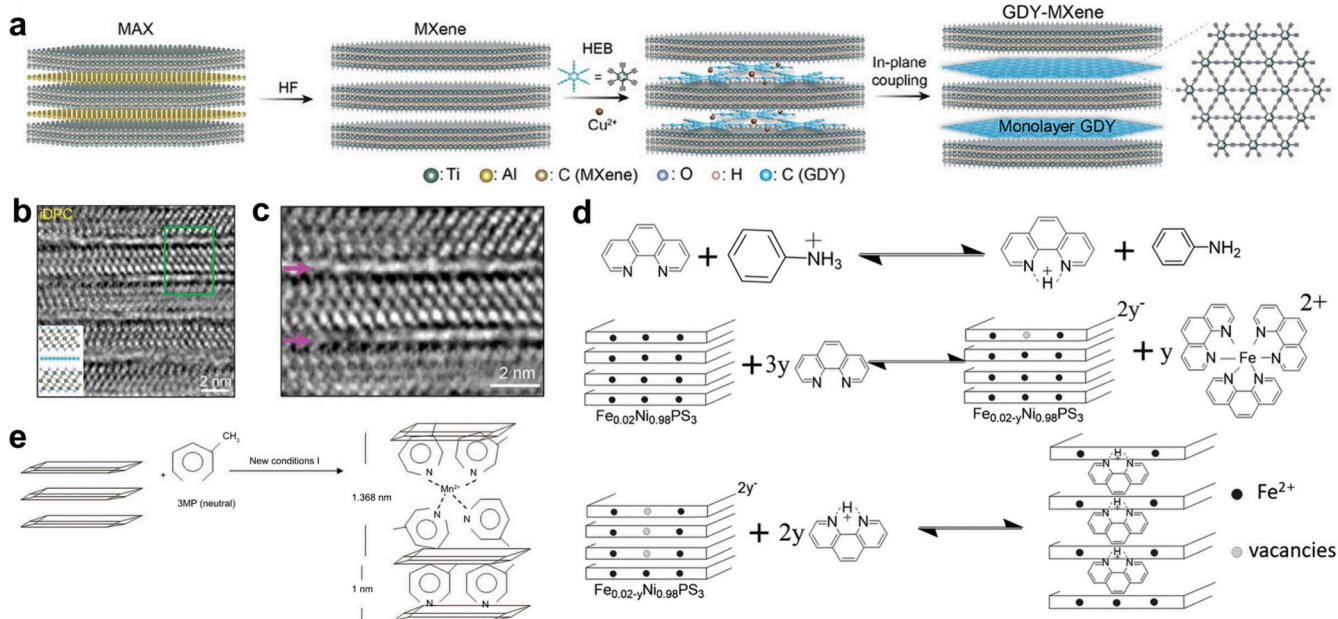


**Figure 13.** Interlayer-confined reactions within vdW gaps. (a) Schematic illustration for the interlayer-confined synthesis of monolayer graphdiyne (GDY) within the vdW gap of MXene. (b) Cross-sectional integrated differential phase-contrast (iDPC)-STEM image of GDY-MXene. (c) Enlarged view of the cyan box in panel (b). Arrows represent monolayer GDY grown within the interlayer space of MXene. (a)–(c) Reproduced from ref 29. Copyright 2024, Wiley. (d) Schematic illustration for three-step reaction mechanism the confined coordination reaction between 1,10-phenanthroline and Fe. Reproduced from ref 124. Copyright 2020, Royal Society of Chemistry. (e) Schematic illustration for the interlayer coordination reaction between 3-methylpyridine and Mn. Reproduced from ref 125. Available under a CC-BY Creative Commons Attribution 4.0 International license (<https://creativecommons.org/licenses/by/4.0/>). Copyright 2009, The Authors, published by Elsevier.

(Figure 11a). These interlayer molecular conformations can be effectively demonstrated by advanced femtosecond broadband sum frequency generation vibrational spectroscopy (SFG-VS). Compared to pristine TaS<sub>2</sub>, these organic–inorganic superlattices exhibits lower thermal conductivity, with a value of 0.426 W m<sup>-1</sup> K<sup>-1</sup> for C12-intercalated TaS<sub>2</sub>, only one-third that of the pristine TaS<sub>2</sub> (Figure 11b). This work highlights the control over molecular configuration as a promising avenue for exploring ultralow thermal conductivity materials.

Organic intercalation plays a crucial role in modulating thermoelectric properties by simultaneously reducing thermal conductivity and increasing electrical conductivity and serves as an ideal tool for enhancing thermoelectric properties. For example, Wang et al.<sup>41</sup> successfully improved the thermoelectric properties of TaS<sub>2</sub> through the intercalation and covalent modification of *tert*-butyl isocyanate. This organic–inorganic hybrid superlattice was obtained by the preintercalation of Li ions followed by guest exchange (Figure 11c). In the side chains covalent modification TaS<sub>2</sub> superlattice, electrical conductivity increased to 3401 S cm<sup>-1</sup>, while the in-plane thermal conductivity decreased to 4.0 W m<sup>-1</sup> K<sup>-1</sup>, representing one-seventh of that of pristine TaS<sub>2</sub>, as shown in Figure 11d,e. Consequently, the ZT value improved to ~0.04 at 443 K (Figure 11f). Importantly, organic intercalation imparts unique molecular characteristics to 2D materials, offering numerous advantages for thermoelectric applications such as diversity and flexibility. A prominent example is the introduction of flexibility in organic-intercalated in TiS<sub>2</sub> (Figure 11g,h), alongside the improvement of thermoelectric properties.<sup>42</sup> Additionally, other organic molecules such as TBA<sup>+</sup> ions, hexylammonium ions, polyethylene glycol and dimethyl sulfoxide can also be intercalated into 2D materials (such as TiS<sub>2</sub>, WSe<sub>2</sub> and

Bi<sub>2</sub>Se<sub>3</sub>), resulting in the enhancement of thermoelectric properties.<sup>72,118–120</sup>

#### 4.4. CISS Effect

Chiral molecules and structures can influence the spin of electrons, resulting in the chirality-induced magnet-free spin generation known as CISS effect.<sup>83–85</sup> Through intercalating chiral molecules into 2D materials, a novel approach has been demonstrated to artificially create chiral solid-state materials.<sup>23,81,121</sup> Furthermore, chiral hybrid superlattices synthesized by organic intercalation typically exhibit high spin selectivity, enhancing the performance of spin filtering devices based on CISS effect.<sup>23,81,121</sup> For instance, the intercalation of chiral right-handed (R-) / left-handed (S-) methylbenzylamine molecules (R-MBA and S-MBA) in 2H-TaS<sub>2</sub> created new chiral superlattices (Figure 12a).<sup>23</sup> When utilized as the spin-filtering layer in spin-selective tunneling junctions (Figure 12b), this superlattice exhibits excellent spin filtering performance, with a tunneling magnetoresistance ratio exceeding 300% and a spin polarization ratio exceeding 60% (Figure 12c,d). This chiral intercalation strategy can be extended to other TMD materials such as TiS<sub>2</sub><sup>81</sup> and MoS<sub>2</sub>.<sup>121</sup> In R-/S-MBA-intercalated MoS<sub>2</sub> and R-/S-PEA (1-(R)-phenethylamine and 1-(S)-phenethylamine molecules)-intercalated TiS<sub>2</sub>, spin polarization ratios of 75% and greater than 90% were observed, respectively. This innovative chiral-molecule intercalation strategy presents new avenues for designing chiral solid-state materials and provides possibilities for developing advanced spintronics devices.

#### 4.5. Interlayer-Confinement Reactions

The vdW gaps between adjacent layers are a subnanometer space, which provides a unique rigid confinement microenvironment for chemical reactions. This space has significant advantages, such as inhibiting agglomeration of reactants and



**Figure 14.** Schematic illustration of a brief overview of organic intercalation and its potential for future advancements.

promoting 2D growth, presenting a new perspective on the atomic-scale fine control of chemical reactions. Li et al.<sup>29</sup> utilized the interlayer vdW gap of MXenes as a reaction space, achieving the synthesis of monolayer graphdiyne (Figure 13a). Within the subnanometer vdW space, *in situ* acetylenic homocoupling of hexaethynylbenzene is produced, which can effectively prevent the material growth along out-of-plane or vertical stacking, thus synthesizing monolayer graphdiyne with micrometer-scale lateral dimensions (Figure 13b,c). The obtained monolayer graphdiyne exhibits excellent electrical properties at room temperature with high electrical conductivity and charge carrier mobility. This work utilized an interlayer-confined synthesis strategy to achieve precise control over 2D materials with precisely controlled layer numbers. Similarly, nitrogen-doped amorphous monolayer carbon can be synthesized through confinement polymerization within the vdW space of layered double hydroxides.<sup>46</sup>

Additionally, confined coordination reactions within vdW gaps have garnered significant research interest.<sup>122–125</sup> Interlayer-confined coordination reactions provide a new approach to modulating the physicochemical properties of 2D materials. A typical example is the interlayer-confined coordination reaction between 1,10-phenanthroline and Fe<sup>2+</sup>. For instance, Ma et al. introduced the complexing agent 1,10-phenanthroline into Fe-doped NiPS<sub>3</sub> (Fe<sub>0.02</sub>Ni<sub>0.98</sub>PS<sub>3</sub>) via a wet chemical method, enabling it to coordinate with Fe.<sup>124</sup> The mechanism of the interlayer-confined coordination reaction between Fe and 1,10-phenanthroline is illustrated in Figure 13d. Through this coordination reaction, the original antiferromagnetic properties are transformed into ferromagnetism with a Curie temperature of ~75 K. Additionally, 3-methylpyridine, as a complexing agent, can participate in interlayer-confined coordination reactions with Mn<sup>2+</sup> within vdW gaps of MnPS<sub>3</sub>, as shown in Figure 13e.<sup>125</sup>

In addition to the properties discussed above, organic intercalation can also modulate other physical phenomena, such as correlated electronic phases, optical properties, and electronic phase transitions.<sup>25</sup> For example, intercalating TBA<sup>+</sup> into VSe<sub>2</sub> can modulate its charge density wave state,<sup>126</sup> and the intercalation of octadecyltrimethylammonium (OTA<sup>+</sup>) and CTA<sup>+</sup> cations in SnS<sub>2</sub> can alter its intrinsic optical properties.<sup>127</sup>

Additionally, the intercalation chemistry in emerging inorganic host systems, such as twisted bilayer systems, beyond conventional layered pristine crystals has attracted widespread interest, offering a new opportunity to advance intercalation chemistry in manipulating quantum materials.<sup>128–130</sup>

## 5. SUMMARY AND PERSPECTIVE

Over 70 years have passed since the initial intercalation of pyridine molecules into TaS<sub>2</sub> to manipulate its superconductivity properties, and the resurgence of interest in organic intercalation in 2D materials after the isolation of graphene<sup>131</sup> has created a wide variety of layered intercalation materials with tunable physicochemical properties. The past two decades have witnessed a prosperity of research focused on organic intercalation. In this review, we present an in-depth overview of organic intercalation for manipulating physicochemical properties, including a summary of various organic guest species (divided into organic cations and organic Lewis base molecules), a discussion on the modulation effects caused by organic intercalation (including dimensionality reduction, interfacial charge transfer, and the impartation of molecular characteristics to 2D materials), and an introduction of the advancements in physicochemical properties modulation through organic intercalation (including topics like superconductivity, magnetism, thermal conductivity and thermoelectricity, CISS effects, and interlayer-confined reactions). We firmly believe that organic intercalation has emerged as a powerful strategy for fine-tuning electronic and atomic structures at the atomic and molecular levels, leading to tunable material properties.

Despite significant progress made in using organic intercalation to alter the physicochemical properties of 2D materials, considerable challenges and opportunities are currently arising in this field. In the following, we will provide a brief overview of organic intercalation, highlighting its potential for future advancements (Figure 14).

- (1) Exploration of the interplay between molecular guest layers and inorganic host layers. Currently, most organic intercalation systems lack significant interplay between the molecular and inorganic layers. The molecular and inorganic layers typically function independently; the

inorganic layers act as electron layers while the molecular layers serve as hole layers, enabling charge doping analogous to metal cation intercalation. However, this independent characteristic limits the exploration of new physical phenomena not present in the inorganic layers. Currently, only a few organic intercalation systems have exhibited interplays between the molecular and inorganic layers, leading to the emergence of new electronic properties such as many-body states<sup>28</sup> and unconventional superconductivity.<sup>27</sup> For example, in chiral-molecule-intercalated TaS<sub>2</sub>, the chiral molecular layers interact with the superconducting TaS<sub>2</sub> layers, leading to chiral superconductivity.<sup>27</sup> In Co(Cp)<sub>2</sub>-intercalated SnSe<sub>2</sub>, the Co(Cp)<sub>2</sub> layers interact with the SnSe<sub>2</sub> layers, resulting in interlayer excitonic insulators.<sup>28</sup> Questions surrounding how interplays occur, when they occur, and the relationship between interplay and new physical properties remain unanswered. Future research should focus on developing new intercalation systems with strong interplays between molecular and inorganic layers to gain a deeper understanding of these phenomena.

- (2) Development of stage ordering intercalation in organic intercalation systems. This stage phenomenon has been extensively studied in inorganic-guest-intercalated systems, such as alkali-metal-ion-intercalated graphite (e.g., Li-intercalated graphite<sup>132</sup>) and metal-chloride-intercalated graphite (e.g., FeCl<sub>3</sub>-intercalated graphite<sup>133</sup>).<sup>134,135</sup> In these inorganic-intercalated graphite compounds, unique intercalation structures, including stage-2 (e.g., C<sub>24</sub>K), stage-3 (e.g., C<sub>36</sub>K), and stage-4 (e.g., C<sub>48</sub>K) intercalation,<sup>135</sup> can be achieved. However, the intercalation of organic species is typically limited to full intercalation along the *c*-axis, that is, stage-1 intercalation, and research on stage intercalation in organic intercalation systems is still lacking. Notably, the stage phenomenon involves controlling the kinetic process of guest intercalation, which depends on various reaction factors. In inorganic intercalation systems, the dynamic processes of inorganic guest intercalation can be controlled to achieve distinct stage orderings by fine-controlling factors including voltage and temperature.<sup>135</sup> On the other hand, organic intercalation systems currently lack effective control mechanisms. Therefore, the development of new organic intercalation systems with controllable stage intercalation is a significant area of research, providing new opportunities for modulating material properties. Additionally, further investigation into the kinetic processes of organic stage intercalation is rare but holds great value for advancing the field.
- (3) Development of interlayer-confined chemical reactions. Nanoconfinement effects on chemical reactivity is a burgeoning area of research, with immense potential for further development and exploration.<sup>136,137</sup> The vdW gap offers a subnanometer space that can serve as a rigid confinement environment for chemical reactions. This confinement space has shown promise in controlling the thickness of 2D materials and enabling the production of atomically thin nanosheets.<sup>29,46</sup> However, the current focus lies on using this rigid interlayer-confined space for self-assembly of intercalated molecules to form ordered molecular structures, and the potential for organic synthesis within this confinement environment remains largely unexplored. Questions arise about the potential of

the interlayer-confined space for organic synthesis: Can it facilitate complex organic synthesis reactions? Is it possible for high-pressure reactions to take place under atmospheric conditions within interlayer-confined space? How can we effectively intercalate multiple organic molecules to promote chemical reactions within the subnanometer transport channels? Additionally, how can inorganic materials be separated from the reaction products? Addressing these questions necessitates further research and exploration, leading to new avenues for innovation and discovery.

- (4) Development of advanced characterization techniques. The detailed analysis of structures and compositions in solid-state materials is crucial for enhancing our understanding of material properties and behaviors. However, confirming the structure of organic-intercalated-hybrid superlattices remains challenging, particularly regarding the interlayer molecule configurations. The molecular structure within hybrid superlattices is often highly sensitive to electron beams; moreover, the molecular sites are less stable and robust than atomic sites in inorganic solids, and certain hybrid superlattices exhibit instability at elevated temperatures or even at room temperature. These challenges complicate the characterization of molecular structures at atomic and molecular levels. For example, directly visualizing the molecular structure using HAADF-STEM is challenging. Furthermore, some characterization techniques do not meet the requirements for *in situ* analysis; for instance, STM necessitates precleavage prior to measurements, potentially leading to deviations from the actual interlayer-confined environment. Therefore, it is imperative to develop new advanced characterization techniques that can accurately delineate the superlattice structure. Exploring nondestructive optical absorption detection technology, such as advanced femtosecond broadband sum frequency generation vibrational spectroscopy (SFG-VS),<sup>117</sup> may represent a promising exploration direction. Additionally, combining theoretical calculations and analyses will be necessary to achieve a clearer structural understanding.

In conclusion, organic molecule intercalation presents a flexible “building block” approach that facilitates the artificial integration of a diverse range of organic molecules with a wide variety of 2D materials, creating numerous organic–inorganic hybrid superlattices with tunable electronic properties and further opening up new avenues for artificially designing new structures. It is anticipated that there will be broader exploration of new intercalation strategies, novel intercalation systems involving new organic molecules, and emergent physical phenomena stemming from organic intercalation, along with more in-depth investigations focusing on the correlation between organic intercalation and the corresponding modulation of physicochemical properties, enhancing our ability and understanding to precisely manipulate material properties.

## AUTHOR INFORMATION

### Corresponding Authors

**Yuqiao Guo** – State Key Laboratory of Precision and Intelligent Chemistry, CAS Key Laboratory of Mechanical Behavior and Design of Materials, University of Science & Technology of

China, Hefei, Anhui 230026, P. R. China; Email: guoyq@ustc.edu.cn

**Changzheng Wu** – State Key Laboratory of Precision and Intelligent Chemistry, CAS Key Laboratory of Mechanical Behavior and Design of Materials, University of Science & Technology of China, Hefei, Anhui 230026, P. R. China; [orcid.org/0000-0002-4416-6358](https://orcid.org/0000-0002-4416-6358); Email: czwu@ustc.edu.cn

## Authors

**Yang Liu** – State Key Laboratory of Precision and Intelligent Chemistry, CAS Key Laboratory of Mechanical Behavior and Design of Materials, University of Science & Technology of China, Hefei, Anhui 230026, P. R. China

**Ziren Wang** – State Key Laboratory of Precision and Intelligent Chemistry, CAS Key Laboratory of Mechanical Behavior and Design of Materials, University of Science & Technology of China, Hefei, Anhui 230026, P. R. China

**Guoliang Hu** – State Key Laboratory of Precision and Intelligent Chemistry, CAS Key Laboratory of Mechanical Behavior and Design of Materials, University of Science & Technology of China, Hefei, Anhui 230026, P. R. China

**Xiaomeng Chen** – State Key Laboratory of Precision and Intelligent Chemistry, CAS Key Laboratory of Mechanical Behavior and Design of Materials, University of Science & Technology of China, Hefei, Anhui 230026, P. R. China

**Ke Xu** – State Key Laboratory of Precision and Intelligent Chemistry, CAS Key Laboratory of Mechanical Behavior and Design of Materials, University of Science & Technology of China, Hefei, Anhui 230026, P. R. China

**Yi Xie** – State Key Laboratory of Precision and Intelligent Chemistry, CAS Key Laboratory of Mechanical Behavior and Design of Materials, University of Science & Technology of China, Hefei, Anhui 230026, P. R. China; [orcid.org/0000-0002-1416-5557](https://orcid.org/0000-0002-1416-5557)

Complete contact information is available at:

<https://pubs.acs.org/10.1021/prechem.4c00084>

## Author Contributions

<sup>§</sup>These authors contributed equally to this work.

## Notes

The authors declare no competing financial interest.

## ACKNOWLEDGMENTS

This work was financially supported by the National Natural Science Foundation of China (21925110, 22321001, 223B1014), the National Key Research and Development Program of China (2022YFA1203600), CAS Project for Young Scientists in Basic Research (YSBR-070), USTC Research Funds of the Double First-Class Initiative (YD2060002004), the Anhui Provincial Natural Science Foundation (2408085J012), Key R&D Program of Shandong Province (2021CXGC010302), Youth Innovation Promotion Association, CAS (2018S00).

## REFERENCES

- (1) Zhou, X.; Shen, Q.; Wang, Y. F.; Dai, Y. F.; Chen, Y. J.; Wu, K. Surface and interfacial sciences for future technologies. *Natl. Sci. Rev.* **2024**, *11* (9), 15.
- (2) Huang, Y. L.; Zheng, Y. J.; Song, Z. B.; Chi, D. Z.; Wee, A. T. S.; Quek, S. Y. The organic-2D transition metal dichalcogenide heterointerface. *Chem. Soc. Rev.* **2018**, *47* (9), 3241–3264.

(3) Piquero-Zulaica, I.; Lobo-Checa, J.; Abd El-Fattah, Z. M.; Ortega, J. E.; Klappenberg, F.; Auwärter, W.; Barth, J. V. Engineering quantum states and electronic landscapes through surface molecular nanoarchitectures. *Rev. Mod. Phys.* **2022**, *94* (4), 045008.

(4) Zhang, T. Y.; Wang, J. T.; Wu, P.; Lu, A. Y.; Kong, J. Vapour-phase deposition of two-dimensional layered chalcogenides. *Nat. Rev. Mater.* **2023**, *8* (12), 799–821.

(5) Novoselov, K. S.; Mishchenko, A.; Carvalho, A.; Neto, A. H. C. 2D materials and van der Waals heterostructures. *Science* **2016**, *353* (6298), 7.

(6) Wu, Y. C.; Li, D. F.; Wu, C. L.; Hwang, H. Y.; Cui, Y. Electrostatic gating and intercalation in 2D materials. *Nat. Rev. Mater.* **2023**, *8* (1), 41–53.

(7) Wu, J. J.; Peng, J.; Sun, H. F.; Guo, Y. Q.; Liu, H. F.; Wu, C. Z.; Xie, Y. Host-guest intercalation chemistry for the synthesis and modification of two-dimensional transition metal dichalcogenides. *Adv. Mater.* **2022**, *34* (28), 2200425.

(8) Yang, R. J.; Mei, L.; Lin, Z. Y.; Fan, Y. Y.; Lim, J.; Guo, J. H.; Liu, Y. J.; Shin, H. S.; Voiry, D.; Lu, Q. Y.; Li, J.; Zeng, Z. Y. Intercalation in 2D materials and in situ studies. *Nat. Rev. Chem.* **2024**, *8* (6), 410–432.

(9) Wan, Z.; Qian, Q.; Huang, Y.; Duan, X. F. Layered hybrid superlattices as designable quantum solids. *Nature* **2024**, *635* (8037), 49–60.

(10) Zhou, J. Y.; Lin, Z. Y.; Ren, H. Y.; Duan, X. D.; Shakir, I.; Huang, Y.; Duan, X. F. Layered intercalation materials. *Adv. Mater.* **2021**, *33* (25), 2004557.

(11) Pereira, J. M.; Tezze, D.; Ormaza, M.; Hueso, L. E.; Gobbi, M. Engineering magnetism and superconductivity in van der Waals materials via organic-ion intercalation. *Adv. Phys. Res.* **2023**, *2* (7), 2200084.

(12) Lin, Y. C.; Torsi, R.; Younas, R.; Hinkle, C. L.; Rigosi, A. F.; Hill, H. M.; Zhang, K. Y.; Huang, S. X.; Shuck, C. E.; Chen, C.; Lin, Y. H.; Maldonado-Lopez, D.; Mendoza-Cortes, J. L.; Ferrier, J.; Kar, S.; Nayir, N.; Rajabpour, S.; van Duin, A. C. T.; Liu, X. W.; Jariwala, D.; Jiang, J.; Shi, J.; Mortelmans, W.; Jaramillo, R.; Lopes, J. M. J.; Engel-Herbert, R.; Trofe, A.; Ignatova, T.; Lee, S. H.; Mao, Z. Q.; Damian, L.; Wang, Y. X.; Steves, M. A.; Knappenberger, K.; Wang, Z. T. Y.; Law, S.; Bepete, G.; Zhou, D.; Lin, J. X.; Scheurer, M. S.; Li, J.; Wang, P. J.; Yu, G.; Wu, S. F.; Akinwande, D.; Redwing, J. M.; Terrones, M.; Robinson, J. A. Recent advances in 2D material theory, synthesis, properties, and applications. *ACS Nano* **2023**, *17* (11), 9694–9747.

(13) Lei, Z. H.; Sathish, C. I.; Geng, X.; Guan, X. W.; Liu, Y. P.; Wang, L.; Qiao, L.; Vinu, A.; Yi, J. B. Manipulation of ferromagnetism in intrinsic two-dimensional magnetic and nonmagnetic materials. *Matter* **2022**, *5* (12), 4212–4273.

(14) Wang, C. S.; You, L.; Cobden, D.; Wang, J. L. Towards two-dimensional van der Waals ferroelectrics. *Nat. Mater.* **2023**, *22* (5), 542–552.

(15) Liu, P. Z.; Wilhams, J. R.; Cha, J. J. Topological nanomaterials. *Nat. Rev. Mater.* **2019**, *4* (7), 479–496.

(16) Ahn, Y.; Lee, G.; Noh, N.; Lee, C.; Le, D. D.; Kim, S.; Lee, Y.; Hyun, J.; Lim, C.; Cha, J.; Jho, M.; Gim, S.; Denlinger, J. D.; Yang, C. H.; Yuk, J. M.; Han, M. J.; Kim, Y. Converting the bulk transition metal dichalcogenides crystal into stacked monolayers via ethylenediamine intercalation. *Nano Lett.* **2023**, *23* (21), 9733–9739.

(17) Burrard-Lucas, M.; Free, D. G.; Sedlmaier, S. J.; Wright, J. D.; Cassidy, S. J.; Hara, Y.; Corkett, A. J.; Lancaster, T.; Baker, P. J.; Blundell, S. J.; Clarke, S. J. Enhancement of the superconducting transition temperature of FeSe by intercalation of a molecular spacer layer. *Nat. Mater.* **2013**, *12* (1), 15–19.

(18) Li, Z. J.; Zhao, Y. C.; Mu, K. J.; Shan, H.; Guo, Y. Q.; Wu, J. J.; Su, Y. Q.; Wu, Q. R.; Sun, Z.; Zhao, A. D.; Cui, X. F.; Wu, C. Z.; Xie, Y. Molecule-confined engineering toward superconductivity and ferromagnetism in two-dimensional superlattice. *J. Am. Chem. Soc.* **2017**, *139* (45), 16398–16404.

(19) Liu, C. C.; Li, Z.; Chen, Z.; Hu, J. Y.; Duan, H. L.; Wang, C.; Feng, S. H.; Liu, R. Q.; Zhang, G. B.; Cao, J. F.; Niu, Y. R.; Li, Q.; Li, P.; Yan, W. S. Realizing room-temperature ferromagnetism in molecular-

- intercalated antiferromagnet VOCl. *Adv. Mater.* **2024**, *36* (35), 2405284.
- (20) Zhang, H. X.; Rousuli, A.; Shen, S. C.; Zhang, K. N.; Wang, C.; Luo, L. P.; Wang, J. Z.; Wu, Y.; Xu, Y.; Duan, W. H.; Yao, H.; Yu, P.; Zhou, S. Y. Enhancement of superconductivity in organic-inorganic hybrid topological materials. *Sci. Bull.* **2020**, *65* (3), 188–193.
- (21) Iturriaga, H.; Martinez, L. M.; Mai, T. T.; Biacchi, A. J.; Augustin, M.; Walker, A. H.; Sanad, M. F.; Sreenivasan, S. T.; Liu, Y.; Santos, E. J. G.; Petrovic, C.; Singamaneni, S. R. Magnetic properties of intercalated quasi-2D  $\text{Fe}_{3-x}\text{GeTe}_2$  van der Waals magnet. *npj 2D Mater. Appl.* **2023**, *7* (1), 56.
- (22) Wang, C.; He, Q. Y.; Halim, U.; Liu, Y. Y.; Zhu, E. B.; Lin, Z. Y.; Xiao, H.; Duan, X. D.; Feng, Z. Y.; Cheng, R.; Weiss, N. O.; Ye, G. J.; Huang, Y. C.; Wu, H.; Cheng, H. C.; Shakir, I.; Liao, L.; Chen, X. H.; Goddard, W. A.; Huang, Y.; Duan, X. F. Monolayer atomic crystal molecular superlattices. *Nature* **2018**, *555* (7695), 231–236.
- (23) Qian, Q.; Ren, H. Y.; Zhou, J. Y.; Wan, Z.; Zhou, J. X.; Yan, X. X.; Cai, J.; Wang, P. Q.; Li, B. L.; Sofer, Z.; Li, B.; Duan, X. D.; Pan, X. Q.; Huang, Y.; Duan, X. F. Chiral molecular intercalation superlattices. *Nature* **2022**, *606* (7916), 902–908.
- (24) Liu, Y. H.; Lv, H. F.; Yuan, B. K.; Liu, Y.; Guo, Y. Q.; Lin, Y.; Tai, X. L.; Qin, Y. L.; Peng, J.; Zhao, J. Y.; Su, Y. Q.; Chen, K.; Chu, W. S.; Yan, W. S.; Wu, X. J.; Wu, C. Z.; Xie, Y. Room-temperature long-range ferromagnetic order in a confined molecular monolayer. *Nat. Phys.* **2024**, *20* (2), 281.
- (25) Xie, Z.; Luo, R.; Ying, T.; Gao, Y.; Song, B.; Yu, T.; Chen, X.; Hao, M.; Chai, C.; Yan, J.; Huang, Z.; Chen, Z.; Du, L.; Zhu, C.; Guo, J.; Chen, X. Dynamic-to-static switch of hydrogen bonds induces a metal-insulator transition in an organic-inorganic superlattice. *Nat. Chem.* **2024**, *16*, 1803–1810.
- (26) Zhang, H. X.; Rousuli, A.; Zhang, K. N.; Luo, L. P.; Guo, C. G.; Cong, X.; Lin, Z. Z.; Bao, C. H.; Zhang, H. Y.; Xu, S. N.; Feng, R. F.; Shen, S. C.; Zhao, K.; Yao, W.; Wu, Y.; Ji, S. H.; Chen, X.; Tan, P. H.; Xue, Q. K.; Xu, Y.; Duan, W. H.; Yu, P.; Zhou, S. Y. Tailored Ising superconductivity in intercalated bulk  $\text{NbSe}_2$ . *Nat. Phys.* **2022**, *18* (12), 1425–1430.
- (27) Wan, Z.; Qiu, G.; Ren, H. Y.; Qian, Q.; Li, Y. C.; Xu, D.; Zhou, J. Y.; Zhou, J. X.; Zhou, B. X.; Wang, L. Y.; Yang, T. H.; Sofer, Z.; Huang, Y.; Wang, K. L.; Duan, X. F. Unconventional superconductivity in chiral molecule- $\text{TaS}_2$  hybrid superlattices. *Nature* **2024**, *632* (8023), 69–74.
- (28) Liu, Y.; Lv, H. F.; Guo, Y. Q.; Zhu, H. E.; Shang, Z. M.; Zhao, Y. C.; Lin, Y.; Tai, X. L.; Guo, Z. Y.; Cui, X. F.; Zhao, J. Y.; Yuan, B. K.; Liu, Y.; Zhang, G. B.; Sun, Z.; Wu, X. J.; Xie, Y.; Wu, C. Z. Interfacial charge-transfer excitonic insulator in a two-dimensional organic-inorganic superlattice. *J. Am. Chem. Soc.* **2024**, *146* (30), 21044–21051.
- (29) Li, J. Q.; Cao, H. C.; Wang, Q. X.; Zhang, H.; Liu, Q.; Chen, C. L.; Shi, Z.; Li, G. X.; Kong, Y.; Cai, Y. C.; Shen, J.; Wu, Y.; Lai, Z. P.; Han, Y.; Zhang, J. Space-confined synthesis of monolayer graphdiyne in mxene interlayer. *Adv. Mater.* **2024**, *36* (7), 2308429.
- (30) Meyer, S. F.; Howard, R. E.; Stewart, G. R.; Acrivos, J. V.; Geballe, T. H. Properties of intercalated 2H- $\text{NbSe}_2$ , 4Hb- $\text{TaS}_2$ , and 1T- $\text{TaS}_2$ . *J. Chem. Phys.* **1975**, *62* (11), 4411–4419.
- (31) Zhao, Y. C.; Su, Y. Q.; Guo, Y. Q.; Peng, J.; Zhao, J. Y.; Wang, C. Y.; Wang, L. J.; Wu, C. Z.; Xie, Y. Quantum Griffiths singularity in a layered superconducting organic-inorganic hybrid superlattice. *ACS Mater. Lett.* **2021**, *3* (2), 210–216.
- (32) Rajapakse, M.; Karki, B.; Abu, U. O.; Pishgar, S.; Musa, M. R. K.; Riyadh, S. M. S.; Yu, M.; Sumanasekera, G.; Jasinski, J. B. Intercalation as a versatile tool for fabrication, property tuning, and phase transitions in 2D materials. *npj 2D Mater. Appl.* **2021**, *5* (1), 30.
- (33) Gamble, F. R.; Disalvo, F. J.; Klemm, R. A.; Geballe, T. H. Superconductivity in layered structure organometallic crystals. *Science* **1970**, *168* (3931), 568–570.
- (34) Morales, J.; Santos, J.; Barrado, J. R. R.; Espinós, J. P.; González-Elipe, A. R. Synthesis and characterization of diamine intercalation compounds of  $\text{SnS}_2$  single crystals. *J. Solid State Chem.* **2000**, *150* (2), 391–398.
- (35) Parry, G. S. Intercalation reactions. *Physica B & C* **1981**, *105* (1–3), 261–267.
- (36) Chen, X. G.; Zhou, H. Q.; Zou, L.; Yang, C. L.; Qin, J. G.; Inokuchi, M. A new organic-inorganic hybrid nanocomposite, BEDT-TTF intercalated into layered  $\text{FePS}_3$ . *J. Incl. Phenom. Macrocycl. Chem.* **2005**, *53*, 205–209.
- (37) Kauzlarich, S. M.; Ellena, J. F.; Stupik, P. D.; Reiff, W. M.; Averill, B. A. Spectroscopic and magnetic properties of  $\text{FeOCl}$  intercalated with organosulfur electron-donors. *J. Am. Chem. Soc.* **1987**, *109* (15), 4561–4570.
- (38) Ma, L. K.; Shi, M. Z.; Kang, B. L.; Peng, K. L.; Meng, F. B.; Zhu, C. S.; Cui, J. H.; Sun, Z. L.; Wang, H. H.; Lei, B.; Wu, T.; Chen, X. H. Quasi-two-dimensional superconductivity in  $\text{SnSe}_2$  via organic ion intercalation. *Phys. Rev. Mater.* **2020**, *4* (12), 124803.
- (39) He, Q. Y.; Lin, Z. Y.; Ding, M. N.; Yin, A. X.; Halim, U.; Wang, C.; Liu, Y.; Cheng, H. C.; Huang, Y.; Duan, X. F. In situ probing molecular intercalation in two-dimensional layered semiconductors. *Nano Lett.* **2019**, *19* (10), 6819–6826.
- (40) Tezze, D.; Pereira, J. M.; Asensio, Y.; Ipatov, M.; Calavalle, F.; Casanova, F.; Bittner, A. M.; Ormaza, M.; Martín-García, B.; Hueso, L. E.; Gobbi, M. Tuning the magnetic properties of  $\text{NiPS}_3$  through organic-ion intercalation. *Nanoscale* **2022**, *14* (4), 1165–1173.
- (41) Wang, S. Z.; Yang, X.; Hou, L. X.; Cui, X. P.; Zheng, X. H.; Zheng, J. Organic covalent modification to improve thermoelectric properties of  $\text{TaS}_2$ . *Nat. Commun.* **2022**, *13*, 4401.
- (42) Wan, C. L.; Gu, X. K.; Dang, F.; Itoh, T.; Wang, Y. F.; Sasaki, H.; Kondo, M.; Koga, K.; Yabuki, K.; Snyder, G. J.; Yang, R. G.; Koumoto, K. Flexible n-type thermoelectric materials by organic intercalation of layered transition metal dichalcogenide  $\text{TiS}_2$ . *Nat. Mater.* **2015**, *14* (6), 622–627.
- (43) Kanatzidis, M. G.; Wu, C. G.; Marcy, H. O.; Degroot, D. C.; Kannewurf, C. R.; Kostikas, A. Intercalation chemistry of conducting polymers - new crystalline microlaminate phases in the polyaniline feocl system. *Adv. Mater.* **1990**, *2* (8), 364–366.
- (44) Matsuo, Y.; Higashika, S.; Kimura, K.; Miyamoto, Y.; Fukutsuka, T.; Sugie, Y. Synthesis of polyaniline-intercalated layered materials via exchange reaction. *J. Mater. Chem.* **2002**, *12* (5), 1592–1596.
- (45) Wang, Y. G.; Wu, W.; Cheng, L.; He, P.; Wang, C. X.; Xia, Y. Y. A polyaniline-intercalated layered manganese oxide nanocomposite prepared by an inorganic/organic interface reaction and its high electrochemical performance for Li storage. *Adv. Mater.* **2008**, *20* (11), 2166–2170.
- (46) Bai, X. H.; Hu, P. F.; Li, A.; Zhang, Y. W.; Li, A. W.; Zhang, G. J.; Xue, Y. F.; Jiang, T. X.; Wang, Z. Z.; Cui, H. K.; Kang, J. X.; Zhao, H. W.; Gu, L.; Zhou, W.; Liu, L. M.; Qiu, X. H.; Guo, L. Nitrogen-doped amorphous monolayer carbon. *Nature* **2024**, *634*, 80–84.
- (47) Liu, X. C.; Zhao, S. Y.; Sun, X. P.; Deng, L. Z.; Zou, X. L.; Hu, Y. C.; Wang, Y. X.; Chu, C. W.; Li, J.; Wu, J. J.; Ke, F. S.; Ajayan, P. M. Spontaneous self-intercalation of copper atoms into transition metal dichalcogenides. *Sci. Adv.* **2020**, *6* (7), No. eaay4092.
- (48) Khan, S.; Aw, E. S. Y.; Nagle-Cocco, L. A. V.; Sud, A.; Ghosh, S.; Subhan, M. K. B.; Xue, Z. K.; Freeman, C.; Sagkovits, D.; Gutiérrez-Llorente, A.; Verzhbitskiy, I.; Arroo, D. M.; Zollitsch, C. W.; Eda, G.; Santos, E. J. G.; Dutton, S. E.; Bramwell, S. T.; Howard, C. A.; Kurebayashi, H. Spin-glass states generated in a van der Waals magnet by alkali-ion intercalation. *Adv. Mater.* **2024**, *36* (36), 10.
- (49) Koski, K. J.; Wessells, C. D.; Reed, B. W.; Cha, J. J.; Kong, D. S.; Cui, Y. Chemical intercalation of zerovalent metals into 2D layered  $\text{Bi}_2\text{Se}_3$  nanoribbons. *J. Am. Chem. Soc.* **2012**, *134* (33), 13773–13779.
- (50) Tezze, D.; Pereira, J. M.; Tutar, D.; Ramos, M.; Regner, J.; Gargiani, P.; Schiller, F.; Casanova, F.; Alegria, A.; Martín-García, B.; Sahin, H.; Sofer, Z.; Ormaza, M.; Hueso, L. E.; Gobbi, M. Tunable magnetism in 2D organic-ion-intercalated  $\text{MnPS}_3$  via molecule-dependent vacancy generation. *Adv. Funct. Mater.* **2024**, 2412771.
- (51) Zhou, J. Y.; Ren, H. Y.; Zhou, J. X.; Wan, Z.; Qian, Q.; Peng, B. S.; Du, S. J.; Yan, X. X.; Pan, X. Q.; Sofer, Z.; Zhang, A.; Huang, Y.; Duan, X. F. Modular assembly of a library of hybrid superlattices and artificial quantum solids. *Matter* **2024**, *7* (3), 1131–1145.
- (52) Li, Z. J.; Zhang, X. Y.; Zhao, X. X.; Li, J.; Herng, T. S.; Xu, H. M.; Lin, F. R.; Lyu, P.; Peng, X. N.; Yu, W.; Hai, X.; Chen, C.; Yang, H. M.; Martin, J.; Lu, J.; Luo, X.; Neto, A. H. C.; Pennycook, S. J.; Ding, J.;

- Feng, Y. P.; Lu, J. Imprinting ferromagnetism and superconductivity in single atomic layers of molecular superlattices. *Adv. Mater.* **2020**, *32* (25), 1907645.
- (53) Zhou, B. X.; Zhou, J. Y.; Wang, L. Y.; Kang, J. H.; Zhang, A.; Zhou, J. X.; Zhang, D. H.; Xu, D.; Hu, B. Y.; Deng, S. B.; Huang, L. B.; Wong, C. W.; Huang, Y.; Duan, X. F. A chemical-dedoping strategy to tailor electron density in molecular-intercalated bulk monolayer MoS<sub>2</sub>. *Nat. Synth.* **2024**, *3* (1), 67.
- (54) Yu, L. X.; Mi, M. J.; Xiao, H.; Wang, S. L.; Sun, Y. T.; Lyu, B. B.; Bai, L. H.; Shen, B.; Liu, M.; Wang, S. P.; Wang, Y. L. Intercalation-induced monolayer behavior in bulk NbSe<sub>2</sub>. *ACS Appl. Mater. Interfaces* **2024**, *16* (43), 59049–59055.
- (55) Ugeda, M. M.; Bradley, A. J.; Zhang, Y.; Onishi, S.; Chen, Y.; Ruan, W.; Ojeda-Aristizabal, C.; Ryu, H.; Edmonds, M. T.; Tsai, H. Z.; Riss, A.; Mo, S. K.; Lee, D. H.; Zettl, A.; Hussain, Z.; Shen, Z. X.; Crommie, M. F. Characterization of collective ground states in single-layer NbSe<sub>2</sub>. *Nat. Phys.* **2016**, *12* (1), 92–97.
- (56) Zong, P. A.; Yoo, D. H.; Zhang, P.; Wang, Y. F.; Huang, Y. J.; Yin, S. J.; Liang, J.; Wang, Y. L.; Koumoto, K.; Wan, C. L. Flexible foil of hybrid TaS<sub>2</sub>/organic superlattice: fabrication and electrical properties. *Small* **2020**, *16* (15), 1901901.
- (57) Wilson, J. A.; Yoffe, A. D. Transition metal dichalcogenides discussion and interpretation of observed optical, electrical and structural properties. *Adv. Phys.* **1969**, *18* (73), 193–335.
- (58) Jiang, S. W.; Shan, J.; Mak, K. F. Electric-field switching of two-dimensional van der Waals magnets. *Nat. Mater.* **2018**, *17* (5), 406–410.
- (59) Jiang, S. W.; Li, L. Z.; Wang, Z. F.; Mak, K. F.; Shan, J. Controlling magnetism in 2D CrI<sub>3</sub> by electrostatic doping. *Nat. Nanotechnol.* **2018**, *13* (7), 549–553.
- (60) Deng, Y. J.; Yu, Y. J.; Shi, M. Z.; Guo, Z. X.; Xu, Z. H.; Wang, J.; Chen, X. H.; Zhang, Y. B. Quantum anomalous Hall effect in intrinsic magnetic topological insulator MnBi<sub>2</sub>Te<sub>4</sub>. *Science* **2020**, *367* (6480), 895–900.
- (61) Navarro-Moratalla, E.; Island, J. O.; Mañas-Valero, S.; Pinilla-Cienfuegos, E.; Castellanos-Gómez, A.; Quereda, J.; Rubio-Bollinger, G.; Chirolli, L.; Silva-Guillén, J. A.; Agrait, N.; Steele, G. A.; Guinea, F.; van der Zant, H. S. J.; Coronado, E. Enhanced superconductivity in atomically thin TaS<sub>2</sub>. *Nat. Commun.* **2016**, *7*, 11043.
- (62) Wang, N. Z.; Shi, M. Z.; Shang, C.; Meng, F. B.; Ma, L. K.; Luo, X. G.; Chen, X. H. Tunable superconductivity by electrochemical intercalation in TaS<sub>2</sub>. *New J. Phys.* **2018**, *20*, 023014.
- (63) Yang, R. J.; Fan, Y. Y.; Mei, L.; Shin, H. S.; Voiry, D.; Lu, Q. Y.; Li, J.; Zeng, Z. Y. Synthesis of atomically thin sheets by the intercalation-based exfoliation of layered materials. *Nat. Synth.* **2023**, *2* (2), 101–118.
- (64) Zeng, L.; Zhang, X.; Liu, Y. N.; Yang, X. X.; Wang, J. H.; Liu, Q.; Luo, Q.; Jing, C. Y.; Yu, X. F.; Qu, G. B.; Chu, P. K.; Jiang, G. B. Surface and interface control of black phosphorus. *Chem.* **2022**, *8* (3), 632–662.
- (65) Ambrosi, A.; Pumera, M. Exfoliation of layered materials using electrochemistry. *Chem. Soc. Rev.* **2018**, *47* (19), 7213–7224.
- (66) Peng, L. L.; Zhu, Y.; Peng, X.; Fang, Z. W.; Chu, W. S.; Wang, Y.; Xie, Y. J.; Li, Y. F.; Cha, J. J.; Yu, G. H. Effective Interlayer Engineering of Two-Dimensional VOPO<sub>4</sub> Nanosheets via Controlled Organic Intercalation for Improving Alkali Ion Storage. *Nano Lett.* **2017**, *17* (10), 6273–6279.
- (67) Zhu, Y.; Peng, L. L.; Fang, Z. W.; Yan, C. S.; Zhang, X.; Yu, G. H. Structural engineering of 2D nanomaterials for energy storage and catalysis. *Adv. Mater.* **2018**, *30* (15), 1706347.
- (68) Zhu, Y.; Qian, Y. M.; Ju, Z. Y.; Peng, L. L.; Yu, G. H. Solvent-dependent intercalation and molecular configurations in metallocene-layered crystal superlattices. *Nano Lett.* **2018**, *18* (9), 6071–6075.
- (69) Zhu, Y.; Ji, Y. J.; Ju, Z. Y.; Yu, K.; Ferreira, P. J.; Liu, Y. Y.; Yu, G. H. Ultrafast intercalation enabled by strong solvent-host interactions: Understanding solvent effect at the atomic level. *Angew. Chem.-Int. Ed.* **2019**, *58* (48), 17205–17209.
- (70) Zhu, Y.; Qian, Y. M.; Ju, Z. Y.; Ji, Y. J.; Yan, Y.; Liu, Y. Y.; Yu, G. H. Understanding charge storage in hydrated layered solids MOPO<sub>4</sub> (M = V, Nb) with tunable interlayer chemistry. *ACS Nano* **2020**, *14* (10), 13824–13833.
- (71) Wang, N.; Mao, N. N.; Wang, Z. E.; Yang, X.; Zhou, X.; Liu, H. N.; Qiao, S. L.; Lei, X. F.; Wang, J. R.; Xu, H.; Ling, X.; Zhang, Q. Y.; Feng, Q. L.; Kong, J. Electrochemical delamination of ultralarge few-layer black phosphorus with a hydrogen-free intercalation mechanism. *Adv. Mater.* **2021**, *33* (1), 2005815.
- (72) Wan, C. L.; Kodama, Y.; Kondo, M.; Sasai, R.; Qian, X.; Gu, X. K.; Koga, K.; Yabuki, K.; Yang, R. G.; Koumoto, K. Dielectric mismatch mediates carrier mobility in organic-intercalated layered TiS<sub>2</sub>. *Nano Lett.* **2015**, *15* (10), 6302–6308.
- (73) Wang, N. Z.; Tang, H. B.; Shi, M. Z.; Zhang, H.; Zhuo, W. Z.; Liu, D. Y.; Meng, F. B.; Ma, L. K.; Ying, J. J.; Zou, L. J.; Sun, Z.; Chen, X. H. Transition from ferromagnetic semiconductor to ferromagnetic metal with enhanced Curie temperature in Cr<sub>x</sub>Ge<sub>2</sub>Te<sub>6</sub> via organic ion intercalation. *J. Am. Chem. Soc.* **2019**, *141* (43), 17166–17173.
- (74) Pereira, J. M.; Tezze, D.; Niehues, I.; Asensio, Y.; Yang, H. Z.; Mester, L.; Chen, S.; Casanova, F.; Bittner, A. M.; Ormaza, M.; Schiller, F.; Martin-García, B.; Hillenbrand, R.; Hueso, L. E.; Gobbi, M. Percolating superconductivity in air-stable organic-ion intercalated MoS<sub>2</sub>. *Adv. Funct. Mater.* **2022**, *32* (52), 2208761.
- (75) Lei, B.; Cui, J. H.; Xiang, Z. J.; Shang, C.; Wang, N. Z.; Ye, G. J.; Luo, X. G.; Wu, T.; Sun, Z.; Chen, X. H. Evolution of high-temperature superconductivity from a low-T<sub>c</sub> phase tuned by carrier concentration in FeSe thin flakes. *Phys. Rev. Lett.* **2016**, *116* (7), 077002.
- (76) Lee, P. A.; Nagaosa, N.; Wen, X. G. Doping a Mott insulator: physics of high-temperature superconductivity. *Rev. Mod. Phys.* **2006**, *78* (1), 17–85.
- (77) Shi, M. Z.; Wang, N. Z.; Lei, B.; Shang, C.; Meng, F. B.; Ma, L. K.; Zhang, F. X.; Kuang, D. Z.; Chen, X. H. Organic-ion-intercalated FeSe-based superconductors. *Phys. Rev. Mater.* **2018**, *2* (7), 074801.
- (78) Mak, K. F.; Shan, J. Opportunities and challenges of interlayer exciton control and manipulation. *Nat. Nanotechnol.* **2018**, *13* (11), 974–976.
- (79) Ma, L. G.; Nguyen, P. X.; Wang, Z. F.; Zeng, Y. X.; Watanabe, K.; Taniguchi, T.; MacDonald, A. H.; Mak, K. F.; Shan, J. Strongly correlated excitonic insulator in atomic double layers. *Nature* **2021**, *598* (7882), 585–589.
- (80) Gupta, S.; Kutana, A.; Yakobson, B. I. Heterobilayers of 2D materials as a platform for excitonic superfluidity. *Nat. Commun.* **2020**, *11* (1), 2989.
- (81) Bian, Z. Y.; Nakano, Y.; Miyata, K.; Oya, I.; Nobuoka, M.; Tsutsui, Y.; Seki, S.; Suda, M. Chiral van der Waals superlattices for enhanced spin-selective transport and spin-dependent electrocatalytic performance. *Adv. Mater.* **2023**, *35* (48), 2306061.
- (82) Glowacki, E. D.; Irimia-Vladu, M.; Bauer, S.; Sariciftci, N. S. Hydrogen-bonds in molecular solids - from biological systems to organic electronics. *J. Mater. Chem. B* **2013**, *1* (31), 3742–3753.
- (83) Bloom, B. P.; Paltiel, Y.; Naaman, R.; Waldeck, D. H. Chiral Induced Spin Selectivity. *Chem. Rev.* **2024**, *124* (4), 1950–1991.
- (84) Bloom, B. P.; Chen, Z. W.; Lu, H. P.; Waldeck, D. H. A chemical perspective on the chiral induced spin selectivity effect. *Natl. Sci. Rev.* **2024**, *11* (9), nwae212.
- (85) Naaman, R.; Paltiel, Y.; Waldeck, D. H. Chiral molecules and the electron spin. *Nat. Rev. Chem.* **2019**, *3* (4), 250–260.
- (86) Chen, Q. J.; Wang, Z. Q.; Boyack, R.; Yang, S. L.; Levin, K. When superconductivity crosses over: from BCS to BEC. *Rev. Mod. Phys.* **2024**, *96* (2), 025002.
- (87) Di Salvo, F. J.; Schwall, R.; Geballe, T. H.; Gamble, F. R.; Osiecki, J. H. Superconductivity in layered compounds with variable interlayer spacings. *Phys. Rev. Lett.* **1971**, *27* (6), 310–313.
- (88) Aoki, R.; Nakamura, S.; Wada, S. Electron-phonon coupling in molecular intercalated niobium disulfide layered compounds. *Synth. Met.* **1983**, *6* (2–3), 193–200.
- (89) Pereira, J. M.; Tezze, D.; Martín-García, B.; Casanova, F.; Ormaza, M.; Hueso, L. E.; Gobbi, M. Enhanced superconductivity in 2H-TaS<sub>2</sub> devices through *in situ* molecular intercalation. *ACS Appl. Mater. Interfaces* **2024**, *16* (31), 41626–41632.

- (90) Orenstein, J.; Millis, A. J. Advances in the physics of high-temperature superconductivity. *Science* **2000**, *288* (5465), 468–474.
- (91) Zhao, J.; Huang, Q.; de la Cruz, C.; Li, S. L.; Lynn, J. W.; Chen, Y.; Green, M. A.; Chen, G. F.; Li, G.; Li, Z.; Luo, J. L.; Wang, N. L.; Dai, P. C. Structural and magnetic phase diagram of CeFeAsO<sub>1-x</sub>F<sub>x</sub> and its relation to high-temperature superconductivity. *Nat. Mater.* **2008**, *7* (12), 953–959.
- (92) Gao, Z.; Zeng, S. Y.; Zhu, B. C.; Li, B. A.; Hao, Q. Y.; Hu, Y. W.; Wang, D. K.; Tang, K. B. A FeSe-based superconductor (C<sub>2</sub>H<sub>8</sub>N<sub>2</sub>)<sub>x</sub>FeSe with only ethylenediamine intercalated. *Sci. China-Mater.* **2018**, *61* (7), 977–984.
- (93) Rendenbach, B.; Hohl, T.; Harm, S.; Hoch, C.; Johrendt, D. Electrochemical synthesis and crystal structure of the organic ion intercalated superconductor (TMA)<sub>0.5</sub>Fe<sub>2</sub>Se<sub>2</sub> with T<sub>c</sub>=43 K. *J. Am. Chem. Soc.* **2021**, *143* (8), 3043–3048.
- (94) Shi, M. Z.; Wang, N. Z.; Lei, B.; Ying, J. J.; Zhu, C. S.; Sun, Z. L.; Cui, J. H.; Meng, F. B.; Hang, C. S.; Ma, L. K.; Chen, X. H. FeSe-based superconductors with a superconducting transition temperature of 50 K. *New J. Phys.* **2018**, *20*, 123007.
- (95) Du, L. J.; Hasan, T.; Castellanos-Gomez, A.; Liu, G. B.; Yao, Y. G.; Lau, C. N.; Sun, Z. P. Engineering symmetry breaking in 2D layered materials. *Nat. Rev. Phys.* **2021**, *3* (3), 193–206.
- (96) Li, J. W.; Li, X. S.; Zhu, H. W. Symmetry engineering in low-dimensional materials. *Mater. Today* **2024**, *75*, 187–209.
- (97) Xi, X. X.; Wang, Z. F.; Zhao, W. W.; Park, J. H.; Law, K. T.; Berger, H.; Forró, L.; Shan, J.; Mak, K. F. Ising pairing in superconducting NbSe<sub>2</sub> atomic layers. *Nat. Phys.* **2016**, *12* (2), 139–143.
- (98) Saito, Y.; Nakamura, Y.; Bahramy, M. S.; Kohama, Y.; Ye, J. T.; Kasahara, Y.; Nakagawa, Y.; Onga, M.; Tokunaga, M.; Nojima, T.; Yanase, Y.; Iwasa, Y. Superconductivity protected by spin-valley locking in ion-gated MoS<sub>2</sub>. *Nat. Phys.* **2016**, *12* (2), 144–149.
- (99) Lu, J. M.; Zheliuk, O.; Leermakers, I.; Yuan, N. F. Q.; Zeitler, U.; Law, K. T.; Ye, J. T. Evidence for two-dimensional Ising superconductivity in gated MoS<sub>2</sub>. *Science* **2015**, *350* (6266), 1353–1357.
- (100) Sukenik, N.; Ozeri, M.; Gutfreund, A.; Fridman, N.; Noah, A.; Yochelis, S.; Remennik, S.; Anahory, Y.; Millo, O.; Paltiel, Y. Imprinting chirality on a conventional superconductor. *Adv. Phys. Res.* **2023**, *2* (4), 2200072.
- (101) Nakajima, R.; Hirobe, D.; Kawaguchi, G.; Nabei, Y.; Sato, T.; Narushima, T.; Okamoto, H.; Yamamoto, H. M. Giant spin polarization and a pair of antiparallel spins in a chiral superconductor. *Nature* **2023**, *613* (7944), 479–484.
- (102) Huang, B.; Clark, G.; Navarro-Moratalla, E.; Klein, D. R.; Cheng, R.; Seyler, K. L.; Zhong, D.; Schmidgall, E.; McGuire, M. A.; Cobden, D. H.; Yao, W.; Xiao, D.; Jarillo-Herrero, P.; Xu, X. D. Layer-dependent ferromagnetism in a van der Waals crystal down to the monolayer limit. *Nature* **2017**, *546* (7657), 270–273.
- (103) Gong, C.; Li, L.; Li, Z. L.; Ji, H. W.; Stern, A.; Xia, Y.; Cao, T.; Bao, W.; Wang, C. Z.; Wang, Y. A.; Qiu, Z. Q.; Cava, R. J.; Louie, S. G.; Xia, J.; Zhang, X. Discovery of intrinsic ferromagnetism in two-dimensional van der Waals crystals. *Nature* **2017**, *546* (7657), 265–269.
- (104) Mermin, N. D.; Wagner, H. Absence of ferromagnetism or antiferromagnetism in one- or 2-dimensional isotropic Heisenberg models. *Phys. Rev. Lett.* **1966**, *17* (22), 1133–1136.
- (105) Li, H.; Ruan, S. C.; Zeng, Y. J. Intrinsic van der Waals magnetic materials from bulk to the 2D limit: new frontiers of spintronics. *Adv. Mater.* **2019**, *31* (27), 1900065.
- (106) Burch, K. S.; Mandrus, D.; Park, J. G. Magnetism in two-dimensional van der Waals materials. *Nature* **2018**, *563* (7729), 47–52.
- (107) Joy, P. A.; Vasudevan, S. The intercalation reaction of pyridine with manganese thiophosphate, MnPS<sub>3</sub>. *J. Am. Chem. Soc.* **1992**, *114* (20), 7792–7801.
- (108) Joy, P. A.; Vasudevan, S. Intercalation of n-alkylamines in FePS<sub>3</sub>. *Chem. Mater.* **1993**, *5* (8), 1182–1191.
- (109) Li, C.; Hu, Z.; Hou, X. F.; Xu, S.; Wu, Z. L.; Du, K. F.; Li, S.; Xu, X. Y.; Chen, Y.; Wang, Z. Y.; Mu, T. C.; Xia, T. L.; Guo, Y. F.; Normand, B.; Yu, W. Q.; Cui, Y. Molecular intercalation in the van der Waals antiferromagnets FePS<sub>3</sub> and NiPS<sub>3</sub>. *Phys. Rev. B* **2024**, *109* (18), 184407.
- (110) Wan, J. Y.; Lacey, S. D.; Dai, J. Q.; Bao, W. Z.; Fuhrer, M. S.; Hu, L. B. Tuning two-dimensional nanomaterials by intercalation: materials, properties and applications. *Chem. Soc. Rev.* **2016**, *45* (24), 6742–6765.
- (111) Samanta, S.; Iturriaga, H.; Mai, T. T.; Biacchi, A. J.; Islam, R.; Fullerton, J.; Walker, A. R. H.; Noufal, M.; Siebenaller, R.; Rowe, E.; Phatak, C.; Susner, M. A.; Xue, F.; Singamaneni, S. R. Spin-phonon coupling and magnetic transition in an organic molecule intercalated Cr<sub>2</sub>Ge<sub>2</sub>Te<sub>6</sub>. *Nano Lett.* **2024**, *24* (30), 9169–9177.
- (112) Mi, M. J.; Zheng, X. W.; Wang, S. L.; Zhou, Y.; Yu, L. X.; Xiao, H.; Song, H. N.; Shen, B.; Li, F.; Bai, L. H.; Chen, Y. X.; Wang, S. P.; Liu, X. H.; Wang, Y. L. Variation between antiferromagnetism and ferrimagnetism in NiPS<sub>3</sub> by electron doping. *Adv. Funct. Mater.* **2022**, *32* (29), 2112750.
- (113) Coronado, E.; Martí-Gastaldo, C.; Navarro-Moratalla, E.; Burzurí, E.; Camón, A.; Luis, F. Hybrid magnetic/superconducting materials obtained by insertion of a single-molecule magnet into TaS<sub>2</sub> layers. *Adv. Mater.* **2011**, *23* (43), 5021–5026.
- (114) Ghosh, T.; Dutta, M.; Sarkar, D.; Biswas, K. Insights into low thermal conductivity in inorganic materials for thermoelectrics. *J. Am. Chem. Soc.* **2022**, *144* (23), 10099–10118.
- (115) Li, Z.; Xiao, C.; Zhu, H.; Xie, Y. Defect Chemistry for Thermoelectric Materials. *J. Am. Chem. Soc.* **2016**, *138* (45), 14810–14819.
- (116) Zhao, C. X.; Li, Z.; Fan, T. J.; Xiao, C.; Xie, Y. Defects engineering with multiple dimensions in thermoelectric materials. *Research* **2020**, *2020*, 9652749.
- (117) Wang, C.; Liu, Y.; Zhu, R. L.; Zhou, T. P.; Wang, M. H.; Cheng, H.; Wang, W. J.; Tai, X. L.; Wang, L.; Chen, L.; Lin, Y.; Ye, S. J.; Xie, Y.; Wu, C. Z. New layered organic-inorganic superlattice with bilayer linear molecules for superhigh heat insulation. *Science China Materials* **2024**, *67*, 4065–4073.
- (118) Wan, C. L.; Tian, R. M.; Kondou, M.; Yang, R. G.; Zong, P. G.; Koumoto, K. Ultrahigh thermoelectric power factor in flexible hybrid inorganic-organic superlattice. *Nat. Commun.* **2017**, *8*, 1024.
- (119) Zong, P. A.; Zhang, P.; Yin, S. J.; Huang, Y. J.; Wang, Y. L.; Wan, C. L. Fabrication and characterization of a hybrid Bi<sub>2</sub>Se<sub>3</sub>/organic superlattice for thermoelectric energy conversion. *Adv. Electron. Mater.* **2019**, *5* (11), 1800842.
- (120) Liang, J.; Li, Y.; Yin, S. J.; Wan, C. L. Flexible organic-intercalated WSe<sub>2</sub> hybrid: electronic structure modification and thermoelectric performance optimization. *Mater. Today Energy* **2023**, *36*, 101355.
- (121) Bian, Z. Y.; Kato, K.; Ogoshi, T.; Cui, Z.; Sa, B. S.; Tsutsui, Y.; Seki, S.; Suda, M. Hybrid chiral MoS<sub>2</sub> Layers for spin-polarized charge transport and spin-dependent electrocatalytic applications. *Adv. Sci.* **2022**, *9* (17), 2201063.
- (122) Clement, R. Intercalation of potentially reactive transition-metal complexes in the lamellar MnPS<sub>3</sub> host lattice. *J. Am. Chem. Soc.* **1981**, *103* (23), 6998–7000.
- (123) Chen, X. G.; Yang, C. L.; Qin, J. G.; Yakushi, K.; Nakazawa, Y.; Ichimura, K. The intercalation reaction of 1,10-phenanthroline with layered compound FePS<sub>3</sub>. *J. Solid State Chem.* **2000**, *150* (2), 258–265.
- (124) Ma, X. P.; Zhang, L.; Xu, C. C.; Dong, Q. X.; Walton, R. I.; Li, Z.; Shi, H. L.; Chen, G. F.; Hu, J. P.; Li, J. Q.; Yang, H. X. The intercalation of 1,10-phenanthroline into layered NiPS<sub>3</sub> via iron dopant seeding. *Chem. Commun.* **2020**, *56* (33), 4603–4606.
- (125) El-Meligi, A. A. New conditions for intercalation of organic compounds into semiconductor nanomaterial. *J. Mater. Sci. Technol.* **2009**, *25* (4), 470–474.
- (126) Meng, F. B.; Liu, Z.; Yang, L. X.; Shi, M. Z.; Ge, B. H.; Zhang, H.; Ying, J. J.; Wang, Z. F.; Wang, Z. Y.; Wu, T.; Chen, X. H. Metal-insulator transition in organic ion intercalated VSe<sub>2</sub> induced by dimensional crossover. *Phys. Rev. B* **2020**, *102* (16), 165410.
- (127) Li, H.; Diao, M. J.; Boukhvalov, D. W.; Ke, Y. T.; Humphrey, M. G.; Zhang, C.; Huang, Z. P. Prominent nonlinear optical absorption in

SnS<sub>2</sub>-based hybrid inorganic-organic superlattice. *Adv. Funct. Mater.* **2024**, *34* (28), 2400077.

(128) Li, B. X.; Wei, J. T.; Jin, C. Q.; Si, K. P.; Meng, L. J.; Wang, X. G.; Jia, Y. Y.; He, Q. Q.; Zhang, P.; Wang, J. L.; Gong, Y. J. Twisted bilayer graphene induced by intercalation. *Nano Lett.* **2023**, *23* (12), 5475–5481.

(129) Larson, D. T.; Carr, S.; Tritsaris, G. A.; Kaxiras, E. Effects of lithium intercalation in twisted bilayer graphene. *Phys. Rev. B* **2020**, *101* (7), 075407.

(130) Wu, Y. C.; Wang, J. Y.; Li, Y. B.; Zhou, J. W.; Wang, B. Y.; Yang, A. K.; Wang, L. W.; Hwang, H. Y.; Cui, Y. Observation of an intermediate state during lithium intercalation of twisted bilayer MoS<sub>2</sub>. *Nat. Commun.* **2022**, *13*, 3008.

(131) Novoselov, K. S.; Geim, A. K.; Morozov, S. V.; Jiang, D.; Zhang, Y.; Dubonos, S. V.; Grigorieva, I. V.; Firsov, A. A. Electric field effect in atomically thin carbon films. *Science* **2004**, *306* (5696), 666–669.

(132) Zhu, X. L.; Su, Z. K.; Tan, R.; Guo, C. L.; Ai, X. P.; Qian, J. F. Scalable synthesis of bilayer graphene at ambient temperature. *J. Am. Chem. Soc.* **2024**, *146* (9), 6388–6396.

(133) Begin, D.; Alain, E.; Furdin, G.; Mareche, J. F. A thermodesorption study of first stage graphite FeCl<sub>3</sub> intercalation compounds. *J. Phys. Chem. Solids* **1996**, *57* (6–8), 849–854.

(134) Stark, M. S.; Kuntz, K. L.; Martens, S. J.; Warren, S. C. Intercalation of layered materials from bulk to 2D. *Adv. Mater.* **2019**, *31* (27), 1808213.

(135) Dresselhaus, M. S.; Dresselhaus, G. Intercalation compounds of graphite. *Adv. Phys.* **1981**, *30* (2), 139–326.

(136) Grommet, A. B.; Feller, M.; Klajn, R. Chemical reactivity under nanoconfinement. *Nat. Nanotechnol.* **2020**, *15* (4), 256–271.

(137) Miners, S. A.; Rance, G. A.; Khlobystov, A. N. Chemical reactions confined within carbon nanotubes. *Chem. Soc. Rev.* **2016**, *45* (17), 4727–4746.